AD NUMBER

AD484795

NEW LIMITATION CHANGE

TO

Approved for public release, distribution unlimited

FROM

Distribution authorized to U.S. Gov't. agencies and their contractors; Administrative/Operational Use; JAN 1966. Other requests shall be referred to US Office of Naval Research, Attn: Mathematical Sciences Division, Washington, DC 20350.

AUTHORITY

ONR notice, 27 Jul 1971

484795

TRG/ A SUBSIDIARY OF CONTROL DATA CORPORATION
ROUTE 110 • MELVILLE, NEW YORK 11749 • 516/531-0600

TRG-156-SR-3

Submitted by:
TRG, Incorporated
A Subsidiary of
Control Data Corporation
Route 110
Melville, New York 11746

NUMERICAL ASPECTS OF WU'S METHOD FOR CAVITATED FLOW, AS APPLIED TO SECTIONS HAVING ROUNDED NOSES

Under Contract No. Nonr-3458(00)

Author: Jerome R. Lurye
Jerome R. Lurye

Approved: Jack Kotik
Jack Kotik

Submitted to:
Scientific Officer
Head, Fluid Dynamics Branch,
Mathematical Sciences Division
Office of Naval Research
Washington, D.C.

January 1966

TABLE OF CONTENTS

LIST OF ILLUSTRATIONS

ACKNOWLEDGEMENT

The author wishes to express his appreciation to Mr. Julian Lustig of TRG, who wrote the computer program and provided much valuable assistance in analyzing the results, and to Dr. Hanan Rubin and Mr. Peter Thomsen who contributed a number of ideas during the early stages of this work.

ABSTRACT

This report describes the main features of a digital computer program for calculating the pressure distribution along bodies in two-dimensional cavity flow in an infinite, incompressible, inviscid fluid. The pressure distribution is used to compute drag, lift, and moment coefficients. The program is based on a theory of cavitated flows developed in recent years by Wu. In the present report, the theory is applied to flow configurations characterized by two fixed detachment points and to sections whose shape in the wetted region is arbitrary, apart from the restriction that there be no sharp corners interior to the wetted region. Calculations are presented for parabolic sections of 10-to-1 fineness ratio and 1-to-1 fineness ratio at several angles-of-attack.

NOMENCLATURE

A = upper detachment point in actual flow; also, a real amplitude associated with the complex velocity potential

A' = upper detachment point in basic flow

B = lower detachment point

B' = lower detachment point in basic flow

C = point of intersection of $\hat{x}$-axis with base of body

C' = point of intersection of $\hat{x}$-axis with base of wedge in basic flow

C_p = pressure coefficient (normalized pressure) = $\frac{p-p_C}{p_S-p_C}$

c_d = drag coefficient = $\frac{F_d}{\frac{1}{2}\rho U^2 \hat{L}}$

c_ℓ = lift coefficient = $\frac{F_\ell}{\frac{1}{2}\rho U^2 \hat{L}}$

c_m = moment coefficient = $\frac{M}{\frac{1}{2}\rho U^2 \hat{L}^2}$

F_d = component, in the direction of the incident stream, of the hydrodynamic force per unit span

F_ℓ = component of same force normal to the incident stream

$f(t,t_o)$ = form of complex velocity potential in the t-plane

$g(t,t_o)$ = $\frac{1}{A} f(t,t_o)$

$h(w)$ = functional relationship between y-coordinate of point on wetted perimeter and auxiliary variable, w

I_j = arc-length integral in w, extending from w_j to w_{j+1}

$I^{(n)}(t')$ = integrand of t'integral in Equation (3.5)

i = subscript denoting i^{th} mesh point; $i = 1,2, \ldots$

$J^{(n)}(t')$ = τ-integral in Equation (3.5)

j = subscript denoting j^{th} mesh or Simpson point; $j = 1,2, \ldots$

$\hat{L}$ = reference length (= $\hat{OC}$ of Figure 2.1) in units of which all normalized lengths are expressed

$\hat{\ell}$ = length of side of wedge in basic flow

M = hydrodynamic moment about point 0

$N(t)$ = $\frac{1}{A}\, s(t)$

N_F = number of fine-mesh intervals in w or t

N_R^+ = number of rough-mesh intervals in w or t on upper profile

$N_R^{(n)-}$ = number of rough-mesh intervals in t on lower profile in the n^{th} iteration

$N_T^{(n)}$ = total number of mesh points in t in n^{th} iteration

n = superscript denoting n^{th} iteration; $n=0,1, \ldots$

0 = nose of body, and origin of $\hat{x}$-$\hat{y}$ coordinate system

P_{RF} = mesh point on upper profile separating rough from fine mesh

P_{FR}^* = provisional point on lower profile separating fine from rough mesh

P_{FR} = final mesh point on lower profile separating fine from rough mesh

p = pressure anywhere on wetted perimeter

p_C = cavity pressure

p_S = stagnation pressure

p_∞ = pressure at infinity

r = real number such that $0 \leq r < 1$

$\hat{S}$ = total length of wetted perimeter

S = $\frac{\hat{S}}{\hat{L}}$

$\hat{s}$ = arc length measured from upper detachment point A to any point on wetted perimeter

$s = \frac{\hat{s}}{L}$

$s(t)$ = s as a function of t

$s^{(n)}(t)$ = approximation to s(t) obtained after n^{th} iteration

$s_j^{(n-1)} = s^{(n-1)}(\tau_{j,n})$

$s[w]$ = s as a function of w

$s_{RF} = s[w_{RF}]$

$s_{FR} = s[w_{FR}]$

t = variable - in general complex - into whose plane the physical plane is mapped so that the complex velocity potential takes the form shown in Equation (2.1). However, in all functions and integrals in this paper, t takes on only real values and is confined to the interval $-1 \leq t \leq 1$.

t_o = image in the t-plane of the point at infinity in the physical plane

$t_o^{(n)}$ = approximation to t_o obtained after n^{th} iteration, $n = 0,1, \ldots$

$t_i^{(n)}$ = i^{th} mesh point in t in n^{th} iteration, $i = 1,2, \ldots$; $n = 0,1, \ldots$

$t_{RF}^{(n)}$ = value of t satisfying equation, $s^{(n-1)}(t) = s_{RF}$

$t_{FR}^{(n)*}$ = value of t satisfying equation, $s^{(n-1)}(t) = s_{FR}$

$t_{FR}^{(n)}$ = the particular $t_i^{(n)}$ lying closest to $t_{FR}^{(n)*}$

$(\Delta t)^{(o)}$ = mesh width in t in basic flow

$(\Delta t)_R^{(n)}$ = width of rough mesh corresponding to the n^{th} iteration

$(\Delta t)_F^{(n)}$ = width of fine mesh corresponding to the n^{th} iteration

U = speed of incident stream

V = $(1+\sigma)^{-\frac{1}{4\epsilon}}$

w = $\pm\sqrt{x}$ = auxiliary variable used in representing the wetted profile

w_i = the i^{th} mesh point in w, $i = 1,2, \ldots$

w_{RF} = $-\sqrt{x_{RF}}$

w_{FR}^* = $\sqrt{x_{FR}^*}$

w_{FR} = the particular w_i lying closest to w_{FR}^*

w_{min} = w_1

w_{max} = $w_{N_R^+ + N_F + N_R^- + 1}$

$(\Delta w)_R$ = width of rough mesh in w

$(\Delta w)_F$ = width of fine mesh in w

$\hat{x}$ = abscissa of arbitrary point on wetted perimeter

x = $\frac{\hat{x}}{\hat{L}}$

x_{RF} = x-coordinate of P_{RF} = $\frac{\hat{x}_{RF}}{\hat{L}}$

x_{FR}^* = x-coordinate of P_{FR}^* = $\frac{\hat{x}_{FR}^*}{\hat{L}}$

x_{FR} = w_{FR}^2

$\hat{y}$ = ordinate of arbitrary point on wetted perimeter

$\hat{z}$ = $\hat{x} + i\hat{y}$

α = angle between incident flow direction and positive $\hat{x}$-axis

β = angle, measured positive counterclockwise, between tangent vector to wetted perimeter and positive $\hat{x}$-axis. Tangent vector points in direction of increasing s.

$\overline{\beta}(s)$ = β expressed as a function of s

δ = relative error

ϵ = fraction of π by which the half-angle of the basic-flow wedge is measured

ρ = density of the fluid

σ = cavitation number = $-\dfrac{p_c - p_\infty}{p_s - p_\infty}$

τ = real integration variable; $-1 \leq \tau \leq 1$

$\tau_{j,n}$ = an Simpson point associated with the τ-integral of Equation (3.5) in the n^{th} iteration.

1. INTRODUCTION AND SUMMARY

As part of an investigation into ventilated flow past surface-piercing struts, TRG has been developing a digital computer program for calculating the pressure distribution along bodies in two dimensional cavity flow in an infinite, incompressible, inviscid fluid. From this pressure distribution we compute the drag coefficient and - in the case of non-zero angle of attack - the lateral or lifting force coefficient and the hydrodynamic moment coefficient. The program is based on a theory of such flows developed in recent years by Wu[1],[2]. As of this writing, we have applied the theory to flow configurations characterized by two fixed detachment points and to sections whose shape in the wetted region is arbitrary, apart from the restriction that there be no sharp corners interior to the wetted region. To the best of our knowledge, Wu's theory has not previously been applied to such problems. Future work may include situations in which one or both detachment points are smooth and/or sharp corners interior to the wetted region are permitted.

In this report we describe the main features of our program, and we exhibit and discuss the computed results obtained thus far in a number of cases. It will be seen that in two of these cases our computational scheme worked well, in one case it gave results whose interpretation we have not yet decided upon, and in one case it was unable to yield meaningful answers. The principle cause of difficulty was probably the insufficient accuracy attained in the evaluation of certain integrals; any further work on the two dimensional problem should therefore include an effort

to improve this accuracy. There is no obstacle other than possibly increased running time, to achieving this higher accuracy.

Before going into details, we summarize the results. Allusions to convergence refer to an iteration procedure which is one of the principal features of the computational scheme, and which is described in Section 3.

Case 1. A 10-to-1 fineness ratio parabola at zero angle-of-attack and zero cavitation number. (See Figure 1.1.) The sequence of computed pressure distributions does not converge. This may be seen from the fact that the first three pressure distributions in the sequence are almost symmetric with respect to the nose of the parabola (the true distribution is symmetric) while the fourth distribution is close to antisymmetric. (See Figure 4.1.) The corresponding values of drag coefficient fluctuate from one iteration to the next in what seems to be a random manner, with a maximum deviation of about 20% above and below the mean for the four iterations.

Case 2. A 1-to-1 parabola at zero angle-of-attack and zero cavitation number. (See Figure 1.2.) Evidence that the sequence of computed pressure distributions converges is provided by the distributions arising from the sixth and seventh iterations, which differ by no more than about 3.5 percent anywhere on the wetted surface, while the corresponding drag coefficients agree to better than a small fraction of a percent. Confirmation of the correctness of the final (seventh) distribution is provided by a comparison with a simple approximate algebraic expression for the pressure along a parabola, derived by Johnson[3]. The agreement

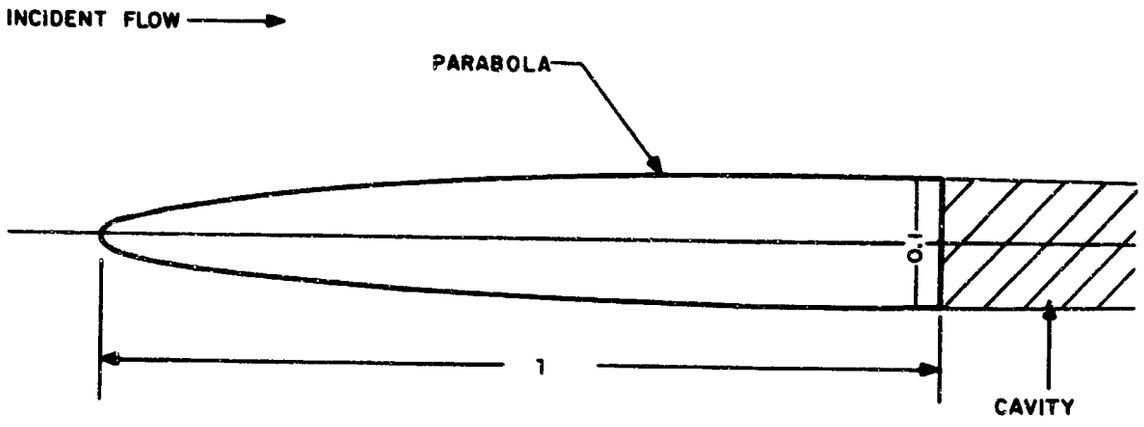

Figure 1.1

10-to-1 PARABOLA, 0° ANGLE-OF-ATTACK

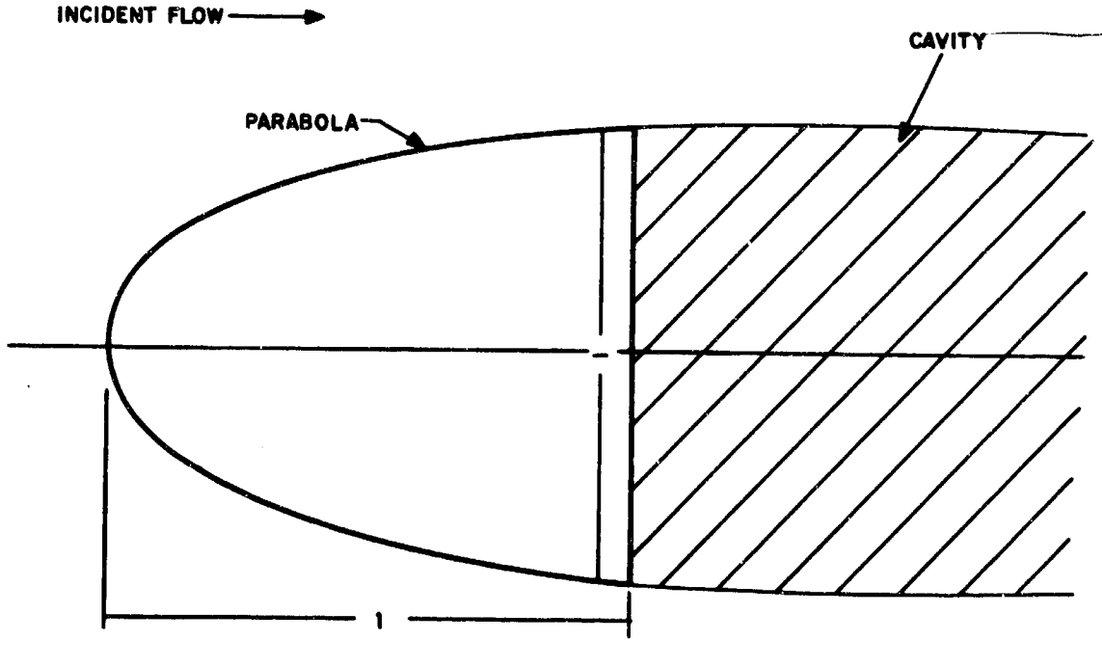

Figure 1.2

1-to-1 PARABOLA, 0° ANGLE-OF-ATTACK

between our result and computations based on Johnson's formula is quite close.

Case 3. A 1-to-1 parabola at 1° angle-of-attack and zero cavitation number. (See Figure 1.3.) Convergence is suggested by the fact that the difference between successive pressure distributions diminishes with iteration number over the entire wetted surface. However, the rate of convergence is slow, and even the thirteenth and fourteenth distributions differ by as much as 15 percent at a point near the nose where the pressure is 40 percent of its stagnation value. Further away from the nose, where the pressure is lower, the difference in the distributions rises to 25 percent. The drag coefficient remains constant over all fourteen iterations, apart from a random fluctuation whose rms value is less than 1 percent. The fluctuation is probably caused by numerical inaccuracies. These inaccuracies have a more serious effect when computing the lateral force and moment coefficients, in which they produce considerably larger fluctuations. The reason for this will be discussed in Section 4.

Case 4. A 1-to-1 parabola at a 5° angle-of-attack and zero cavitation number. (See Figure 1.4.) In this case, after fourteen iterations there is no indication of convergence to a limiting pressure distribution. On the other hand, all of the distributions are similar in form. Moreover, apart from the third distribution, which has a large negative dip, the pressure distributions fall within a range of values such that any one of them appears physically reasonable. This suggests that the failure to converge is a numerical phenomenon, an idea that is reinforced by the fact

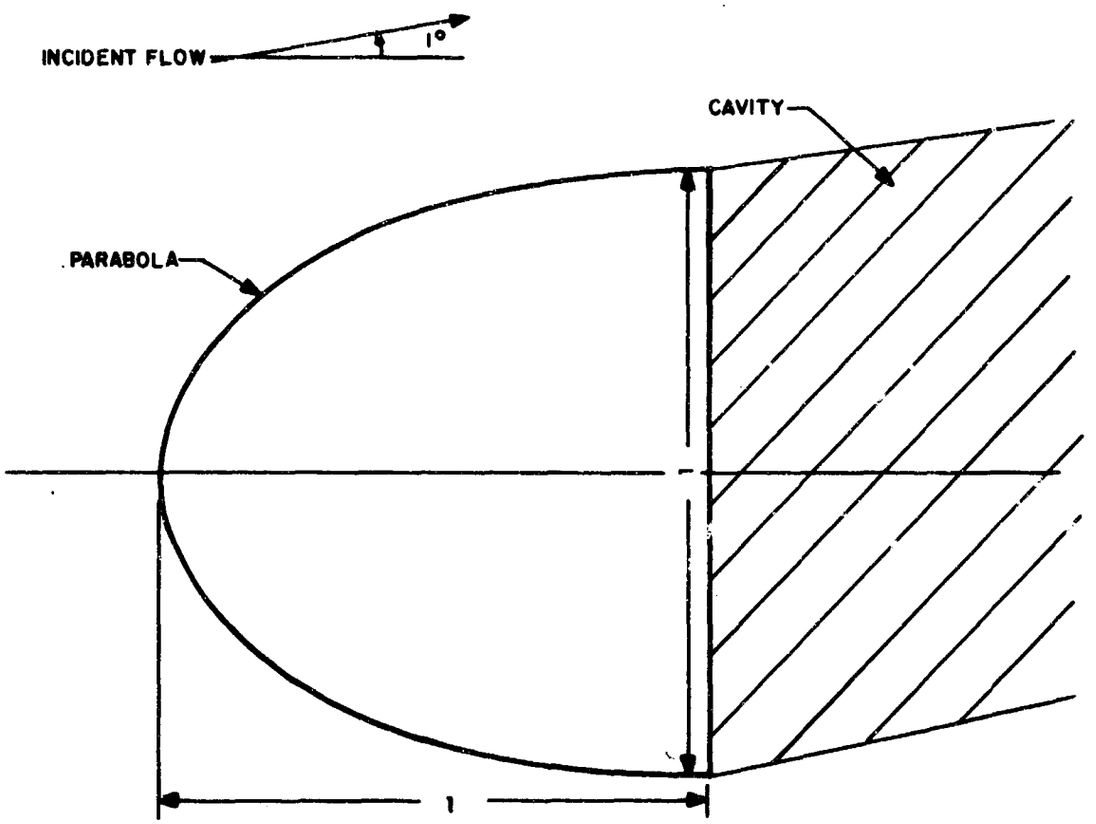

Figure 1.3
1-to-1 PARABOLA, 1° ANGLE-OF-ATTACK

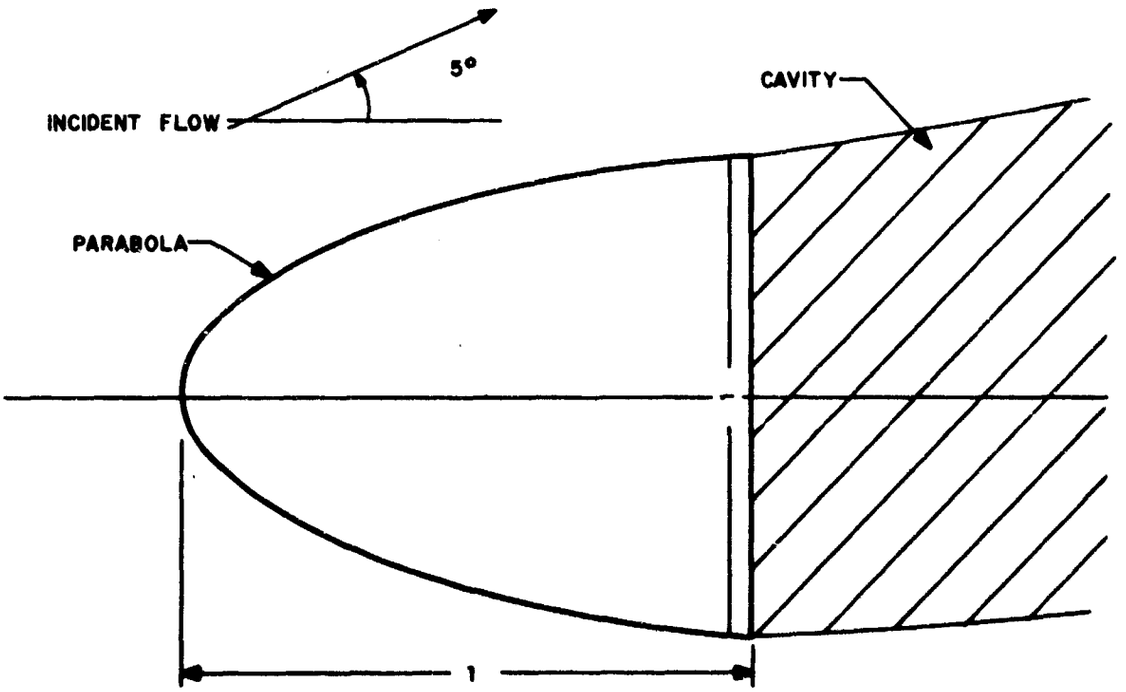

Figure 1.4

1-to-1 PARABOLA, 5° ANGLE-OF-ATTACK

that, as in the 1° case, the drag coefficient varies in what appears to be a random manner as a function of iteration number. Although the fluctuation of the drag coefficient about its mean value is larger than in the 1° case, it is still small, having an rms value of 4 to 5 percent. Also as in the 1° case, the fluctuations of the lift and moment coefficients are considerably larger than those of the drag coefficient, for reasons to be discussed in Section 4.

It should be remarked that the computation time in all four cases averaged to somewhat less than 0.01 hours per iteration on the IBM 7094 computer.

To render intelligible the computational procedure for calculating the pressure distribution on the body, and the corresponding drag, lift, and moment coefficients, it is necessary to give a brief account of the underlying theory. Accordingly, the next section contains such an account. In Section 3, we describe the computational scheme itself. Although we do not exhibit the actual computer program, we do explain all procedures called for in the program specification, other than standard subroutines. In Section 4, we present some of the numerical results obtained for the aforementioned cases. Finally, Section 5 lists some recommendations for future improvements in the computational procedure.

2. OUTLINE OF THEORY

The configuration under discussion is shown in Figure 2.1.

In the figure, AOBA represents the perimeter of the body upon which is incident a uniform flow of complex velocity $Ue^{-i\alpha}$. The shaded region represents the cavity, the points A and B being the fixed detachment points from which emanate the two free (constant pressure) streamlines that bound the cavity. O, the origin of the $\hat{x}$-$\hat{y}$ coordinate system, is generally placed most conveniently at the point of maximum curvature of the perimeter; for the usual bodies this point is well defined. It is convenient, also, to have the $\hat{y}$-axis tangent to the perimeter at O. $P(\hat{s})$ is any running point on the perimeter, where $\hat{s}$ is the arc length from A to P. β is the angle, measured positive counterclockwise, between the positive $\hat{x}$-direction and the tangent vector at P. This vector points in the direction of increasing $\hat{s}$. The significance of the points P_{RF}, P^*_{FR}, and P_{FR} with abscissae $\hat{x}_{RF}$, $\hat{x}^*_{FR}$, and $\hat{x}_{FR}$ will be explained presently.

As mentioned, our computation procedure is based on a theory due to Wu[1],[2] wherein the region of potential flow exterior to the body and cavity in the physical ($\hat{z}=\hat{x}+i\hat{y}$) plane* is mapped conformally into the interior of a slitted semicircle in the plane of a new complex variable denoted by t. (Here, t has no connection with the time.) This mapping has the property

*In Wu's mapping, the origin of the rectangular coordinate system in the physical plane is at A, but this has no effect on the equations needed in the present work.

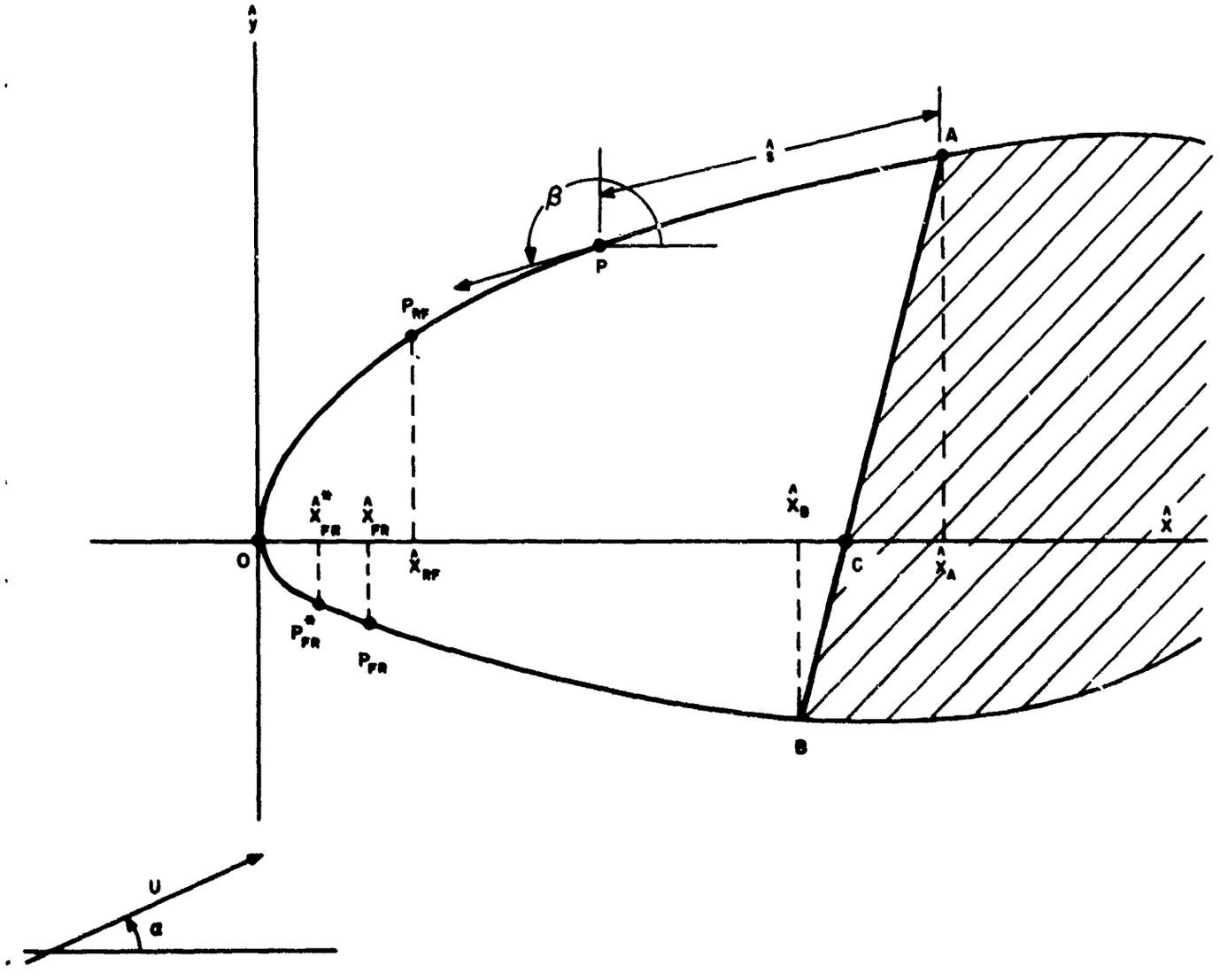

Figure 2.1

GENERAL CONFIGURATION UNDER DISCUSSION

that the velocity potential in the complex t plane, call it $f(t,t_o)$, takes the form of an elementary algebraic function of t, viz.,

$$f(t,t_o) = At^2\left[(t-t_o)(t-\bar{t}_o)(t-t_o^{-1})(t-\bar{t}_o^{-1})\right]^{-1} \qquad (2.1)$$

where t_o is the image, in the t-plane, of the point $\hat{z}=\infty$, A is a real constant (not to be confused with point A of Figure 2.1) to be determined, and the bar (in this case) denotes the complex conjugate.

Naturally, the complex function that accomplishes the mapping is not known in advance, and its determination constitutes the main problem. However, if as in our case, one is not attempting to obtain the entire flow but only the pressure distribution on the body, one can get by with the computation of a good deal less than the entire mapping function.

The base of the semi-circle in the t-plane is the interval $-1 \leq t \leq 1$ on the real t-axis, and this interval is also the image in the t-plane of the wetted perimeter AOB of the body. Thus as t goes from -1 to 1, P goes from A to B via O, while $\hat{s}$ varies from 0 to $\hat{S}$, where $\hat{S}$ is the length of the wetted perimeter. As will become evident, the determination of the unknown function $\hat{s}(t)$ is an essential step in obtaining the pressure distribution on the body.

Before writing expressions for these quantities, we introduce certain normalizations into the problem. Specifically, we normalize all lengths with respect to some convenient length, $\hat{L}$, defined in the plane of the flow. $\hat{L}$ in our case is taken to

be $\widehat{OC}$, the length of $\hat{x}$-axis intercepted by the body. Then, if s represents normalized arc length, $s = \frac{\hat{s}}{\hat{L}}$. Likewise, all other normalized lengths are denoted by removing the hat symbol from the corresponding letter. Further, we normalize all velocity magnitudeswith respect to the constant speed of the fluid along the free streamlines that bound the cavity. Finally, we introduce three dimensionless coefficients, viz., a two-dimensional drag coefficient, c_d, a two-dimensional lateral force or lift coefficient, c_ℓ, and a two-dimensional moment coefficient, c_m. These are defined as follows:

$$c_d = \frac{F_d}{\frac{1}{2}\rho U^2 \hat{L}} \tag{2.2a}$$

$$c_\ell = \frac{F_\ell}{\frac{1}{2}\rho U^2 \hat{L}} \tag{2.2b}$$

$$c_m = \frac{M}{\frac{1}{2}\rho U^2 \hat{L}^2} \tag{2.3}$$

where F_d is the component, in the direction of the incident stream, of the hydrodynamic force per unit span acting on the body, F_ℓ is the component of the same force normal to the stream, and M is the moment (measured positive counterclockwise) of that force about the nose, O. U is the unnormalized speed of the incident stream and ρ is the fluid density.

Instead of the pressure itself, it is convenient to compute the dimensionless pressure coefficient, C_p, defined by

$$C_p = \frac{p-p_C}{p_S-p_C} \tag{2.4}$$

where p is the fluid pressure anywhere along the perimeter of the body, p_C is the pressure in the cavity, and p_S is the stagnation pressure. It can be shown that the drag, lift, and moment coefficients are then expressible in terms of C_p by means of the relationships

$$c_d = c_x \cos\alpha + c_y \sin\alpha \tag{2.5a}$$

$$c_\ell = - c_x \sin\alpha + c_y \cos\alpha \tag{2.5b}$$

$$c_m = (1+\sigma) \int_0^S C_p(s)\left[x(s)\cos\bar{\beta}(s)+y(s)\sin\bar{\beta}(s)\right] ds \tag{2.5c}$$

where

$$c_x = - (1+\sigma) \int_0^S C_p(s) \sin\bar{\beta}(s) ds \tag{2.6a}$$

$$c_y = (1+\sigma) \int_0^S C_p(s) \cos\bar{\beta}(s)\, ds \tag{2.6b}$$

In these equations, α is the angle, measured positive counterclockwise, between the incident flow velocity and the positive x-axis, S is the normalized length of the wetted perimeter and σ is the cavitation number, defined by

$$\sigma = - \frac{p_c-p_\infty}{p_S-p_\infty} \tag{2.7}$$

where p_∞ is the fluid pressure at infinity. $\bar{\beta}(s)$ denotes the functional dependence of the angle β on the arc length s, while x(s) and y(s) denote the corresponding dependences of the x and

y coordinates of a point on the perimeter. These functional dependences are known, being determined solely by the geometry of the body.

Next we change the integration variable from s to t. It is shown in Wu[1],[2] that $C_p[t]$, defined as $C_p(s(t))$, can be written

$$C_p[t] = 1 - \left[\frac{f_t(t,t_o)}{s_t(t)}\right]^2 \qquad -1 \leq t \leq 1 \tag{2.8}$$

In Eq. (2.8), $f(t,t_o)$ is the image in the t-plane of the normalized velocity potential (see Equation (2.1)), $s(t)$ is the still-to-be-determined normalized arc length as a function of t, and the subscript t denotes differentiation with respect to t.

Changing from s to t in Eq. (2.5c), (2.6), and (2.7) and using Eq. (2.8), we see that these equations can be written in the form

$$c_x = -(1+\sigma)\int_{-1}^{1}\left\{1-\left[\frac{f_t(t,t_o)}{s_t(t)}\right]^2\right\}\sin\bar{\beta}(s(t))\,s_t(t)\,dt \tag{2.9a}$$

$$c_y = (1+\sigma)\int_{-1}^{1}\left\{1-\left[\frac{f_t(t,t_o)}{s_t(t)}\right]^2\right\}\cos\bar{\beta}(s(t))\,s_t(t)\,dt \tag{2.9b}$$

$$c_m = (1+\sigma)\int_{-1}^{1}\left\{1-\left[\frac{f_t(t,t_o)}{s_t(t)}\right]^2\right\}\Big[x(s(t))\cos\bar{\beta}(s(t)) + y(s(t))\sin\bar{\beta}(s(t))\Big]\,s_t(t)\,dt \tag{2.10}$$

Equations (2.8), (2.9a and b), and (2.10) combined with Eq. (2.5a and b) show that once the function s(t) has been determined, the desired pressure distribution coefficient, $C_p(s)$, and the drag, lift, and moment coefficients c_d, c_ℓ, and c_m can be inferred by direct calculation.

We now invoke one of the main results in Wu's work[2], viz., that the unknown function s(t) is the solution to a nonlinear integral equation, viz.,

$$s(t) = \int_{-1}^{t} \exp\left\{\frac{1-t'^2}{\pi} \int_{-1}^{1} \frac{\bar{\beta}(s(\tau)) - \bar{\beta}(s(t'))}{(\tau - t')(\tau t' - 1)} d\tau\right\} f_{t'}(t', t_o) \frac{dt'}{t'} \qquad (2.11)$$

where $f(t,t_o)$ is given by Eq. (2.1), with the real constant, A, and the complex constant, t_o, still to be determined. It will be recalled that t_o is the image in the t-plane of the point $z=\infty$. Imposition of the condition that the complex velocity $\to Ue^{-i\alpha}$ as $z\to\infty$ leads to the following equation for t_o:

$$t_o = \frac{e^{-i\alpha}}{\sqrt{1+\sigma}} \exp\left\{\frac{1-t_o^2}{\pi} \int_{-1}^{1} \frac{\bar{\beta}(s(\tau))}{(\tau - t_o)(\tau t_o - 1)} d\tau\right\} \qquad (2.12)$$

Finally, if S is the (given) normalized length of the wetted perimeter, we have

$$s(1) = S \qquad (2.13)$$

The function s(t) and the constants A and t_o are to be obtained by solving Equations (2.11), (2.12), and (2.13) simultaneously. It is this solution process which we carry out numerically and for which we have developed the computational procedure described in the next section.

3. COMPUTATIONAL PROCEDURE

To calculate the solution to Equations (2.11)-(2.13), we use the method of successive iterations. For this purpose, it is convenient to write Equations (2.11) and (2.13) in a slightly altered form. We put

$$f(t,t_o) = Ag(t,t_o) \tag{3.1}$$

and

$$s(t) = AN(t) \tag{3.2}$$

where $g(t,t_o)$ is the algebraic function multiplying the constant A in Eq. (2.1).

Equation (2.11) then becomes

$$N(t) = \int_{-1}^{t} \exp\left\{\frac{1-t'^2}{\pi}\int_{-1}^{1}\frac{\bar{\beta}(s(\tau))-\bar{\beta}(s(t'))}{(\tau-t')(\tau t'-1)}\,d\tau\right\} g_{t'}(t',t_o)\,\frac{dt'}{t'} \tag{3.3}$$

while for Eq. (2.13), we get

$$A = \frac{S}{N(1)} \tag{3.4}$$

There are many ways in which to start off the iteration process. We have followed Wu in introducing the idea of the "basic flow." This is a known two-dimensional cavitated flow about some body which ideally - but not necessarily - has a close resemblance to the given body. From this known basic flow, one can obtain the starting quantities or zeroth iterates, $s^{(o)}(t)$ and $t_o^{(o)}$*. $s^{(o)}(t)$ and $t_o^{(o)}$ are substituted into the right side of Eq. (3.3) to yield $N^{(1)}(t)$, from which $A^{(1)}$ is then calculated

*Since we start off with $s^{(o)}(t)$ rather than $N^{(o)}(t)$, we do not need the zeroth iterate, $A^{(o)}$.

via Eq. (3.4). Likewise $t_o^{(1)}$ is obtained by substitution of $s^o(t)$ and $t_o^{(o)}$ into the right side of Eq. (2.12). Finally, $s^{(1)}(t) = A^{(1)}N^{(1)}(t)$, in accordance with Eq. (3.2).

The formalities of going from the $(n-1)^{st}$ to the n^{th} iterate are defined by the following equations:

$$N^{(n)}(t) = \int_{-1}^{t} \exp\left\{\frac{1-t'^2}{\pi}\int_{-1}^{1}\frac{\bar{\beta}\left(s^{(n-1)}(\tau)\right) - \bar{\beta}\left(s^{(n-1)}(t')\right)}{(\tau-t')(\tau t'-1)}d\tau\right\} g_{t'}(t', t_o^{(n-1)})\frac{dt'}{t'} \tag{3.5}$$

$$A^{(n)} = \frac{S}{N^{(n)}(1)} \tag{3.6}$$

$$s^{(n)}(t) = A^{(n)}N^{(n)}(t) \tag{3.7}$$

$$t_o^{(n)} = \frac{e^{-i\alpha}}{\sqrt{1+\sigma}} \exp\left\{\frac{1-(t_o^{(n-1)})^2}{\pi}\int_{-1}^{1}\frac{\bar{\beta}\left(s^{(n-1)}(\tau)\right)d\tau}{(\tau-t_o^{(n-1)})(\tau t_o^{(n-1)}-1)}\right\} \tag{3.8}$$

To these, we may add equations for the pressure coefficient and the drag, lift, and moment coefficients, quantities which although not iterated in themselves, are to be calculated at the end of each iteration. We have from Eq. (2.8)

$$C_p^{(n)}[t] = 1 - \left[\frac{f_t(t, t_o^{(n)})}{s_t^{(n)}(t)}\right]^2 \tag{3.9}$$

while from Eq. (2.5a and b), (2.9a and b), and (2.10) we get

$$c_d^{(n)} = c_x^{(n)}\cos\alpha + c_y^{(n)}\sin\alpha \tag{3.10a}$$

$$c_\ell^{(n)} = -c_x^{(n)}\sin\alpha + c_y^{(n)}\cos\alpha \tag{3.10b}$$

$$c_x^{(n)} = -(1+\sigma)\int_{-1}^{1}\left\{1-\left[\frac{f_t(t,t_o^{(n)})}{s_t^{(n)}(t)}\right]^2\right\}\sin\bar{\beta}(s^{(n)}(t))\,s_t^{(n)}(t)\,dt \qquad (3.11)$$

$$c_y^{(n)} = (1+\sigma)\int_{-1}^{1}\left\{1-\left[\frac{f_t(t,t_o^{(n)})}{s_t^{(n)}(t)}\right]^2\right\}\cos\bar{\beta}(s^{(n)}(t))\,s_t^{(n)}(t)\,dt \qquad (3.12)$$

$$c_m^{(n)} = (1+\sigma)\int_{-1}^{1}\left\{1-\left[\frac{f_t(t,t_o^{(n)})}{s_t^{(n)}(t)}\right]^2\right\}\Big[x(s^{(n)}(t))\cos\bar{\beta}(s^{(n)}(t)) + y(s^{(n)}(t))\sin\bar{\beta}(s^{(n)}(t))\Big]\,s_t^{(n)}(t)\,dt \qquad (3.13)$$

As of this writing, we have not investigated the theoretical convergence of the foregoing sequences. However, such convergence seems likely when the choice of basic flow is not too unreasonable, and indeed there is numerical evidence of convergence in certain of the specific cases to be described. At any rate, we shall assume that if the zeroth order iterates are suitably chosen, the sequences defined by Equations (3.5)-(3.12) do, in fact, converge. Note that even when this assumption is correct, it does not follow that the numerical realizations of these sequences converge, since purely numerical phenomena such as accumulation of errors may intervene to spoil the convergence.

The actual computation divides itself logically into four stages:

a) numerical specification of the body geometry,

b) basic flow calculation,

c) numerical realization of the iteration procedure, and

d) calculation of the pressure coefficient and the drag,

lift, and moment coefficients from Eq. (3.7) and Eq. (3.9)-(3.13). We describe each of these in turn.

A. Specification of the Body Geometry

The body geometry enters into the foregoing equations through the functions $\bar{\beta}(s)$, $x(s)$, and $y(s)$. We first relate these functions analytically to the usual x-y equations of the body profile. We then define a set of data points along the perimeter at which $\bar{\beta}(s)$, $x(s)$, and $y(s)$ are to be evaluated.

Let the body shape in the wetted region be specified originally by two single valued functions, viz.,

$$\hat{y} = \hat{y}^{+}(\hat{x}) \qquad \text{upper profile} \qquad (\hat{y} > 0) \tag{3.14a}$$

$$\hat{y} = \hat{y}^{-}(\hat{x}) \qquad \text{lower profile} \qquad (\hat{y} < 0) \tag{3.14b}$$

which, upon the introduction of $\hat{\ell}$ as the unit of length*, become

$$y = y^{+}(x) \qquad y > 0 \tag{3.15a}$$

$$y = y^{-}(x) \qquad y < 0 \tag{3.15b}$$

These functions are to be continuously differentiable except at the nose, where the profile has a vertical tangent. Under the assumption that the nose is parabolic, it is convenient to introduce a new variable, w, related to x by the equations

$$w = -\sqrt{x} \qquad \text{upper profile} \qquad (y > 0) \tag{3.16a}$$

$$w = \sqrt{x} \qquad \text{lower profile} \qquad (y < 0) \tag{3.16b}$$

We then have instead of Equations (3.15), the single equation

$$y = h(w) \qquad w_{min} \leq w \leq w_{max} \tag{3.17}$$

*We recall that $\hat{\ell} = \overline{OC}$, the length of $\hat{x}$-axis intercepted by the body; see Figure 2.1.

where

$$h(w) = y^{\pm}(w^2), \qquad w \lesseqgtr 0 \tag{3.18}$$

The quantities w_{min} and w_{max} are defined by

$$w_{min} = -\sqrt{x_A} \tag{3.19}$$

$$w_{max} = \sqrt{x_B} \tag{3.20}$$

where x_A and x_B are the x-coordinates of the detachment points A and B shown in Figure 2.1. In these equations, the positive square root is intended.

Because the nose is parabolic, the function h(w) is continuously differentiable throughout the interval $w_{min} < w < w_{max}$. Thus the function g(w), defined by

$$g(w) = \frac{dh}{dw}, \tag{3.21}$$

is continuous in that same interval.

The arc length s can be expressed as a function of w as follows:

$$s[w] = \int_{w_{min}}^{w} \sqrt{\left(\frac{dx}{dw'}\right)^2 + \left(\frac{dy}{dw'}\right)^2}\, dw' \tag{3.22}$$

Substituting from Equations (3.16) and (3.21) into Equation (3.22), we get

$$s[w] = \int_{w_{min}}^{w} \sqrt{(2w')^2 + [g(w')]^2}\, dw' \tag{3.23}$$

Finally, from the definition of the angle β of Figure 2.1, it follows that β is related to the derivative $\frac{dx}{ds}$ by the equations

$$\beta = 2\pi - \arccos \frac{dx}{ds}, \quad g(w) \leq 0, \; w \lesseqgtr 0 \tag{3.24}$$

$$\beta = \arccos \frac{dx}{ds}, \quad g(w) > 0, \; w < 0 \tag{3.25}$$

$$\beta = 2\pi + \arccos \frac{dx}{ds}, \quad g(w) > 0, \; w > 0 \tag{3.26}$$

Here the arc cosine means the single valued inverse cosine function whose range extends from 0 to π. It is necessary always to express β in terms of this particular branch of the inverse cosine since it is only this branch that the computer subroutine calculates.

From Equations (3.16) and (3.23) we substitute for dx and ds in Equations (3.24)-(3.26) to obtain

$$\beta = 2\pi - \arccos \frac{2w}{\sqrt{(2w)^2+[g(w)]^2}}, \; g(w) \leq 0, \; w \lesseqgtr 0 \tag{3.27}$$

$$\beta = \arccos \frac{2w}{\sqrt{(2w)^2+[g(w)]^2}}, \; g(w) > 0, \; w < 0 \tag{3.28}$$

$$\beta = 2\pi + \arccos \frac{2w}{\sqrt{(2w)^2+[g(w)]^2}}, \; g(w) > 0, \; w > 0 \tag{3.29}$$

By means of Equations (3.16), (3.17), (3.21), (3.23), and (3.27)-(3.29) we have expressed each of the variables x, y, s, and β as a function of w alone. Thereby x, y, and β are determined as functions of s, a fact which we use later in the program when carrying out the iteration procedure.

We now define, along the wetted perimeter of the body, a set of data points at which x, y, β, and s are to be evaluated. Because on the actual profiles of interest, β changes very rapidly as a function of s or w in the vicinity of the nose and very slowly elsewhere, we distribute the data points with two different densities. In the vicinity of the nose a high density or fine mesh is used; elsewhere we use a low density or rough mesh. Let P_{RF} and P^*_{FR} be those points on the upper and lower profiles that separate the part of the perimeter over which β changes rapidly from the rest. The points are indicated in Figure 2.1, where their abscissas are denoted by $\hat{x}_{RF}$ and $\hat{x}^*_{FR}$. For a given profile these points - and therefore the values of $\hat{x}_{RF}$ and $\hat{x}^*_{FR}$ - are chosen by eye. In the discussion which follows it will become evident that in general only one of the two points can be a data point (mesh point), and we arbitrarily take this one to be P_{RF}, the point on the upper profile. We denote by P_{FR} the mesh point lying closest to P^*_{FR} on the side toward the point B. The quantitative specification of P_{FR} will be given presently.

Corresponding to the normalized x-values we define the w-values

$$w_{RF} = -\sqrt{x_{RF}} \tag{3.30}$$

$$w^*_{FR} = \sqrt{x^*_{FR}} \tag{3.31}$$

Similarly, we can write

$$w_{FR} = \sqrt{x_{FR}} \tag{3.32}$$

but this equation, unlike the previous two, does not provide a definition of the quantity on its left-hand side because x_{FR} is

as yet unknown. In fact, as we shall see, w_{FR} is obtained first, whence x_{FR} can be calculated from Equation (3.32), if desired.

Let w_i be the w-value of the i^{th} mesh point, counting w_{min} as w_1. Then from the definitions of the mesh points P_{RF} and P_{FR}, we have the scheme:

$$w_{min} \leq w_i < w_{RF} \qquad \text{rough mesh} \qquad (3.33)$$

$$w_{RF} \leq w_i \leq w_{FR} \qquad \text{fine mesh} \qquad (3.34)$$

$$w_{FR} \leq w_i \leq w_{max} \qquad \text{rough mesh} \qquad (3.35)$$

Now choose a value for N_R^+, the number of rough-mesh intervals on the upper profile. Since w_{min} and w_{RF} are already defined by Equations (3.19) and (3.30), the choice of N_R^+ fixes the value of $(\Delta w)_R$, the length of the rough-mesh interval in w. Specifically,

$$(\Delta w)_R = \frac{w_{RF} - w_{min}}{N_R^+} \qquad (3.36)$$

With $(\Delta w)_R$ thus determined, we see that N_R^-, the number of rough-mesh intervals on the lower profile, cannot be arbitrary but follows from (3.35) and the definition of P_{FR}. We have in fact

$$\frac{w_{max} - w_{FR}^*}{(\Delta w)_R} = N_R^- + r, \quad 0 \leq r < 1 \qquad (3.37)$$

which says that N_R^- is the integer part of the left side of Equation (3.37). This determination of N_R^- then leads at once to the desired expression for w_{FR}, viz.,

$$w_{FR} = w_{max} - N_R^-(\Delta w)_R \qquad (3.38)$$

Finally, we choose a value for N_F, the number of fine-mesh intervals*. From Equations (3.30) and (3.38) we can then calculate $(\Delta w)_F$, the length of the fine-mesh interval. We have

$$(\Delta w)_F = \frac{w_{FR} - w_{RF}}{N_F} \tag{3.39}$$

The foregoing equations now enable us to write the following expressions for the calculation of w_i, the w-value of the i^{th} mesh point. We recall that $w_1 = w_{min} = -\sqrt{x_A}$.

$$w_i = -\sqrt{x_A} + (i-1)(\Delta w)_R \qquad i = 1,2,\ldots N_R^+ \tag{3.40}$$

$$w_i = w_{RF} + (i - N_R^+ - 1)(\Delta w)_F \tag{3.41}$$

$$= -\sqrt{x_A} + N_R^+(\Delta w)_R + (i - N_R^+ - 1)(\Delta w)_F$$

$$i = N_R^+ + 1, \cdots\cdots N_R^+ + N_F$$

$$w_i = w_{FR} + (i - N_R^+ - N_F - 1)(\Delta w)_R \tag{3.42}$$

$$= -\sqrt{x_A} + N_R^+(\Delta w)_R + N_F(\Delta w)_F$$

$$+ (i - N_R^+ - N_F - 1)(\Delta w)_R$$

$$i = N_R^+ + N_F + 1, \cdots\cdots N_R^+ + N_F + N_R^- + 1$$

Next we evaluate the functions $x(w)$, $h(w)$, $s[w]$, and $\bar{\beta}(w)$ at the points w_i defined by Equations (3.40)-(3.42). From Equations (3.16), $x(w_i) = w_i^2$, while $h(w_i)$ is evaluated via Equations (3.17) and (3.18), $s[w_i]$ via Equation (3.23), and $\bar{\beta}(w_i)$ via Equations (3.27)-(3.29). We should note that for the

*When the body is symmetric in y - a common occurrence - it is convenient to have the nose point, 0, be one of the mesh points, w_i. Accordingly, we always make N_F an even number.

profiles in which we are presently interested, the functions $y^{\pm}(x)$ - and therefore $h(w)$ - are simple combinations of elementary functions so that the evaluation of $h(w_i)$ presents no problem. The function $g(w)$ appearing in Equations (3.23) and (3.27)-(3.29) and defined as $\frac{dh}{dw}$, is evaluated by first differentiating $h(w)$ analytically and then computing the resulting expression at the desired value of w.

To evaluate the integral on the right of Equation (3.23), we first observe that

$$s[w_i] = \sum_{j=1}^{i-1} I_j \qquad i = 2,3, \ldots . \tag{3.43}$$

where I_j stands for the integral from w_j to w_{j+1}. For computational purposes, it is advantageous to express Equation (3.43) in recursive form, viz.,

$$s[w_{i+1}] = s[w_i] + I_i \qquad i = 1,2, \ldots . \tag{3.44}$$

with $$s[w_1] = 0.$$

For any given i, the integral I_i in Equation (3.44) is calculated repeatedly by means of Simpson's rule, the number of Simpson subintervals doubling at each repetition. The process stops when successive computed values of I_i differ by less than some preassigned fractional amount, in our case 0.1%.

This completes the description of Part A of our program, viz., the specification of the body geometry (profile calculation). We conclude with a recapitulation of the input and output variables for Part A.

Inputs for Part A

$\hat{L}$, $\hat{x}_A$, $\hat{x}_B$, $\hat{x}_{RF}$, $\hat{x}^*_{FR}$, N_R^+, N_F, Equations $\hat{y} = \hat{y}^+(\hat{x})$, $\hat{y} = \hat{y}^-(\hat{x})$

Outputs from Part A

w_i, $i = 1,2, \ldots N_R^+ + N_F + N_R^- + 1$, $x(w_i)$, $h(w_i)$,

$s[w_i]$, $\bar{\beta}(w_i)$.

In addition to being stored for use in the rest of the program, these five variables are printed out to expedite program analysis and checking.

B. Basic Flow Calculation

As already mentioned, we use some known flow, the so-called "basic flow," to furnish the zeroth order quantites, $s^{(o)}(t)$ and $t_o^{(o)}$, with which the iteration process is started. The choice of the basic flow is made on the dual grounds of ease of calculation and a presumed resemblance to the flow around the body of interest. In this subsection we exhibit, by way of illustration, one such basic flow, and we show how it leads to the numerical specification of the zeroth order iterates.

In the case in question - and, for that matter, in all the cases thus far computed - the original body is a parabola located symmetrically with respect to the x-axis. The base AB of the body - see Figure (2.1) - is normal to the $\hat{x}$-axis so that $x_B = x_A$, while from symmetry we have $y_B = - y_A$. We assume an incident flow parallel to the $\hat{x}$-axis, i.e., $\alpha=0$.

For a basic flow we choose the flow about a wedge with sides of length $\hat{\ell}$ located symmetrically with respect to the $\hat{x}$-axis

and having its vertex at 0 (see Figure 3.1). This flow has the merit that its s(t) function is known explicitly [2]. As with the parabola, the base A'B' of the wedge is normal to the $\hat{x}$-axis, while the incident flow is parallel to that axis. The fixed detachment points of the basic flow are at A' and B' corresponding to the values t=-1 and t=1, respectively, in the t-plane. The half-angle of the wedge at 0 is denoted by $\epsilon\pi$ with $0 < \epsilon < \frac{1}{2}$.

To coordinate the wedge dimensions and the basic flow parameters with the parabola and its flow, we proceed as follows: we set the length of the base A'B' of the wedge equal to that of the parabola, AB. This gives the cavities in the two flows the same initial widths. Next we require that the wetted perimeters of the two bodies have the same lengths, i.e.,

$$2\hat{\ell} = \hat{S} \tag{3.45}$$

These two conditions fix the angle $\epsilon\pi$ since we have

$$\epsilon\pi = \arcsin \frac{\hat{A'C'}}{\hat{\ell}} \tag{3.46}$$

Further, the cavitation number σ is assumed to be the same in both flows. Then, since the velocity magnitudes are normalized to the free streamline speeds in both flows, the normalized incident flow speeds must be equal and in fact are given by

$$U = \frac{1}{\sqrt{1+\sigma}} \tag{3.47}$$

Finally, all lengths in both flows are normalized with respect $\hat{L}$ (= $\hat{OC}$ of Figure 2.1).

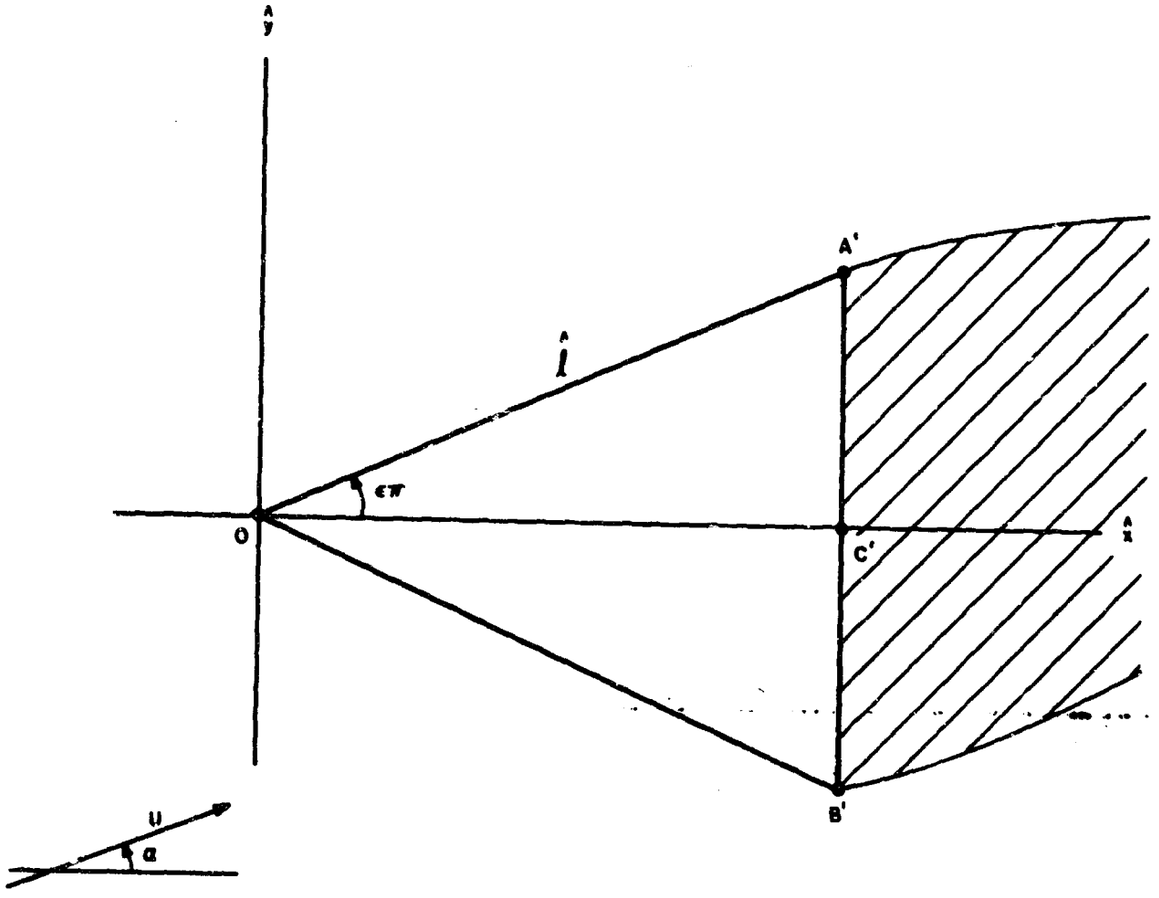

Figure 3.1

BASIC-FLOW CONFIGURATION

The quantities $s^{(o)}(t)$ and $t_o^{(o)}$, arising from the wedge flow and serving as zeroth order iterates in the parabola flow, can now be written down from Wu's solution to the wedge problem [2]. Specifically,

$$s^{(o)}(t) = \ell - s_w(-t) \qquad -1 \leq t < 0 \tag{3.48}$$

$$s^{(o)}(t) = \ell + s_w(t) \qquad 0 \leq t \leq 1 \tag{3.49}$$

where the function $s_w(t)$ is defined by

$$s_w(t) = \ell \frac{t^{2(1-\epsilon)}(t^2+V^2)^{-1}(t^2+V^{-2})^{-1} + 2\epsilon\int_0^t t'^{1-2\epsilon}(t'^2+V^2)^{-1}(t'^2+V^{-2})^{-1}dt'}{V^2(1+V^2)^{-2} + 2\epsilon\int_0^1 t'^{1-2\epsilon}(t'^2+V^2)^{-1}(t'^2+V^{-2})^{-1}dt'} \tag{3.50}$$

In Equation (3.50), the constant V is

$$V = (1+\sigma)^{-\frac{1}{4\epsilon}} \tag{3.51}$$

It will be recalled that ϵ, the coefficient of π in Equation (3.46), is restricted to the interval $0 < \epsilon < \frac{1}{2}$.

Note also that $s_w(t)$ is defined only for $t \geq 0$.

From Wu's solution, the constant $t_o^{(o)}$ is given by

$$t_o^{(o)} = -iV \tag{3.52}$$

Next we represent $s^{(o)}(t)$ numerically. For this purpose we establish, over the interval $-1 \leq t \leq 1$, a set of equally spaced mesh points at which $s^{(o)}(t)$ is to be evaluated. The number of such points is chosen equal to the number of mesh

points in w, i.e., $N_R^+ + N_F + N_R^- + 1$. Since the t-points are equally spaced*, it follows that the mesh width is given by

$$(\Delta t)^o = \frac{2}{N_R^+ + N_F + N_R^-} \tag{3.53}$$

where the superscript o stands for zeroth iteration.

Denoting the i^{th} mesh point in the zeroth iteration by $t_i^{(o)}$ with $t_1^{(o)} = -1$, we have

$$t_i^{(o)} = -1 + (i-1)(\Delta t)^o \qquad i=1,2, \ldots N_R^+ + N_F + N_R^- + 1 \tag{3.54}$$

or, in view of Equation (3.53),

$$t_i^{(o)} = -1 + \frac{2(i-1)}{N_R^+ + N_F + N_R^-} \qquad i=1,2, \ldots N_R^+ + N_F + N_R^- + 1 \tag{3.55}$$

We now compute $s^{(o)}(t_i^{(o)})$ and $t_o^{(o)}$ via Equations (3.48)-(3.50), (3.52), and (3.55). It should be remarked that the evaluation of the integrals in Equation (3.50) is carried out according to the scheme already described in connection with the integral of Equation (3.23).

Inputs for Part B

$$\hat{L},\ \hat{AB},\ \hat{S},\ N_R^+,\ N_F,\ N_R^-,\ \sigma$$

Outputs from Part B

$$t_i^{(o)},\ s^{(o)}(t_i^{(o)}) \qquad i=1,2, \ldots N_R^+ + N_F + N_R^- + 1,\ t_o^{(o)}.$$

*This single-density mesh is used only in representing the zeroth order iterate, $s^{(o)}(t)$. When computing $s^{(n)}(t)$, $n \geq 1$, we distribute the mesh points over the interval $-1 \leq t \leq 1$ with two densities, in much the same manner and for the same reason as was done with the w-points of the profile calculation. This is discussed more fully in the next subsection.

C. Numerical Realization of the Iteration Process

We have already mentioned that the mesh points at which the n^{th} iterate $s^{(n)}(t)$, $n \geq 1$, is to be evaluated are distributed on the interval $-1 \leq t \leq 1$ with two densities (rough and fine mesh) in analogy with the mesh points in w. Unlike the w-points, however, the mesh points in t change from one iteration to the next; so also does the number of mesh points. Accordingly, we denote the t-value of the i^{th} mesh point in the n^{th} iteration by $t_i^{(n)}$, $i=1,2, \ldots N_T^{(n)}$ ($t_1^{(n)}=-1$), where $N_T^{(n)}$ is the number of mesh points used in the n^{th} iteration.

As the first step in explaining how the numbers, $t_i^{(n)}$, are arrived at, we describe the procedure for calculating $t_{RF}^{(n)}$ and $t_{FR}^{(n)}$, $n \geq 1$; these are defined as the mesh points in t at which, with increasing t, the mesh changes from rough to fine and fine to rough, respectively. That is, they are the analogies of w_{RF} and w_{FR} except for the dependence on iteration number. The calculation of $t_{RF}^{(n)}$ and $t_{FR}^{(n)}$ is recursive since it presumes that the mesh points $t_i^{(n-1)}$ have already been established.

Let s_{RF} and s_{FR} be the arc lengths at which the w-mesh density changes. We may write

$$s_{RF} = s[w_{RF}] \tag{3.56}$$

$$s_{FR} = s[w_{FR}] \tag{3.57}$$

where it will be recalled that the values of the function on the right of these equations form part of the output of Part A. It is important to note that since $s(w_i)$ depends only on the geometry of the body, the quantities s_{RF} and s_{FR} are independent of the

iteration number. Next consider the (n-1)st iterate $s^{(n-1)}(t)$. We choose as $t_{RF}^{(n)}$ the value of t that satisfies the equation

$$s^{(n-1)}(t) = s_{RF} \tag{3.58}$$

Since the representation of $s^{(n-1)}(t)$ is numerical - it is defined by the sequence of calculated values $s^{(n-1)}(t_i^{(n-1)})$, $i=1,2, \ldots N_T^{(n-1)}$ - we must solve Equation (3.58) by interpolation among these calculated values. We use a Lagrange four-point interpolation scheme as a subroutine for the numerical solution of Equation (3.58).

With $t_{RF}^{(n)}$ computed, we choose a value for the number of rough-mesh intervals in t on the upper profile. It is convenient to make this number equal to its counterpart in the case of the w-mesh, viz., N_R^+. Note that this particular number characterizing the t-mesh is then independent of n. We can now write

$$(\Delta t)_R^{(n)} = \frac{t_{RF}^{(n)} - t_1^{(n)}}{N_K^+} = \frac{t_{RF}^{(n)}+1}{N_R^+} \tag{3.59}$$

where $(\Delta t)_R^{(n)}$ is the width of the rough-mesh interval corresponding to the n^{th} iteration.

Before calculating $t_{FR}^{(n)}$, we introduce a quantity $t_{FR}^{(n)*}$. This is defined as the value of t satisfying

$$s^{(n-1)}(t) = s_{FR} \tag{3.59a}$$

The remarks pertaining to Equation (3.58) apply to this equation as well. In particular, the solution is effected via the same Lagrange interpolation process.

Note that in general $t_{FR}^{(n)*}$ is not one of the mesh points in t.

We now pick the mesh point $t_{FR}^{(n)}$ as follows: starting at the point $t_{N_T}^{(n)}(=1)$, we lay off in the direction of decreasing t a rough mesh of width $(\Delta t)_R^{(n)}$, where $(\Delta t)_R^{(n)}$ is given by Equation (3.59). From the mesh points thus generated, we choose as $t_{FR}^{(n)}$ the one lying closest to $t_{FR}^{(n)*}$ (If $t_{FR}^{(n)*}$ is - to within the number of significant figures retained - precisely midway between two mesh points, then the mesh point with the less positive t- value is taken to be $t_{FR}^{(n)}$.) If $N_R^{(n)}$ denotes the number of rough-mesh intervals on the lower profile in the n^{th} iteration, it can be shown that the analytic representation of the procedure just described is given by the equation

$$\frac{t_{N_T}^{(n)} - t_{FR}^{(n)*} + \frac{1}{2}}{(\Delta t)_R^{(n)}} = \frac{\frac{3}{2} - t_{FR}^{(n)*}}{(\Delta t)_R^{(n)}} = N_R^{(n)-} + r \qquad (3.60)$$

$$0 \leq r < 1$$

where the first equality follows from the fact that $t_{N_T}^{(n)} = 1$. The second equation states that $N_R^{(n)-}$ is the integer part of the expression on the left. This determination of $N_R^{(n)-}$ leads at once to the desired expression for $t_{FR}^{(n)}$ (cf. Equation (3.38) for w_{FR}):

$$\begin{aligned} t_{FR}^{(n)} &= t_{N_T}^{(n)} - N_R^{(n)-}(\Delta t)_R^{(n)} \\ &= 1 - N_R^{(n)-}(\Delta t)_R^{(n)} \end{aligned} \qquad (3.61)$$

Next, we choose the number of fine-mesh intervals in t to equal N_F, the number of such intervals in w. As in the case of N_R^+, this number is independent of n. From the meaning of $t_{RF}^{(n)}$ and $t_{FR}^{(n)}$ together with their calculated values as given by Equations (3.58) and (3.61), we can then write for $(\Delta t)_F^{(n)}$, the width of the fine-mesh interval

$$(\Delta t)_F^{(n)} = \frac{t_{FR}^{(n)} - t_{RF}^{(n)}}{N_F} \tag{3.62}$$

The foregoing equations now enable us to use the following expressions for the calculation of the quantities $t_i^{(n)}$. We recall that $t_1^{(n)} = -1$.

$$t_i^{(n)} = -1 + (i - 1)(\Delta t)_R^{(n)} \qquad i = 1,2, \ldots N_R^+ \tag{3.63}$$

$$\begin{aligned} t_i^{(n)} &= t_{RF}^{(n)} + (i - N_R^+ - 1)(\Delta t)_F^{(n)} \\ &= -1 + N_R^+(\Delta t)_R^{(n)} + (i - N_R^+ - 1)(\Delta t)_F^{(n)} \end{aligned} \tag{3.64}$$

$$i = N_R^+ + 1, \ldots N_R^+ + N_F$$

$$\begin{aligned} t_i^{(n)} &= t_{FR}^{(n)} + (i - N_R^+ - N_F - 1)(\Delta t)_R^{(n)} \\ &= -1 + N_R^+(\Delta t)_R^{(n)} + N_F(\Delta t)_F^{(n)} \\ &\quad + (i - N_R^+ - N_F - 1)(\Delta t)_R^{(n)} \end{aligned} \tag{3.65}$$

$$i = N_R^+ + N_F + 1, \ldots N_T^{(n)}$$

where $N_T^{(n)} = N_R^+ + N_F + N_R^{(n)-} + 1$.

With the mesh points $t_i^{(n)}$ established, we can discuss the computation of the n^{th} order quantities $s^{(n)}(t_i^{(n)})$ and $t_o^{(n)}$ via the iteration Equations (3.5) - (3.8). The principal task is to perform numerically the integrations occurring in those equations. This is a complex operation having a number of aspects which we now discuss.

1. Consider first the integral over t', the "outer integral" of Equation (3.5). Since the function $N^{(n)}(t)$ - and therefore $s^{(n)}(t)$, see Equation (3.7) - is to be evaluated at the points $t_i^{(n)}$ given by Equations (3.63) - (3.65), it follows that the upper limit, t, of the outer integral is to be assigned the values $t_i^{(n)}$ only. Now it turns out that the integrand - call it $I^{(n)}(t')$ - of the outer integral is a smooth function* of t', and therefore we save a great deal of machine time without much loss of accuracy by evaluating $I^{(n)}(t')$ only at the points $t' = t_i^{(n)}$. The integrals

$$N^{(n)}(t_i^{(n)}) = \int_{-1}^{t_i^{(n)}} I^{(n)}(t')dt' \qquad i = 1,2, \ldots N_T^{(n)} \quad (3.66)$$

are then computed by a recursion scheme almost identical to that defined by Equation (3.44). The only difference is that in the

---

* This may not be true in the neighborhood of t'=0 for the 10-to-1 parabola at zero angle-of-attack. See the discussion of Case 1 in Section 4.

present case the integrand $I^{(n)}(t')$ is given in tabular form rather than analytically; thus the values of $I^{(n)}(t')$ required by the Simpson's rule subroutine* must be obtained by interpolation among the quantities $I^{(n)}(t_i^{(n)})$. For this purpose, as with all our interpolations, the Lagrange four-point procedure is used.

2. We can write $I^{(n)}(t')$ as

$$I^{(n)}(t') = \exp\left[\frac{1-t'^2}{\pi} J^{(n)}(t')\right] g_{t'}(t;t_o^{(n-1)}) \frac{1}{t^\tau} \tag{3.67}$$

where $J^{(n)}(t')$ represents the "inner integral"

$$J^{(n)}(t') = \int_{-1}^{1} \frac{\bar{\beta}(s^{(n-1)}(\tau)) - \bar{\beta}(s^{(n-1)}(t'))}{(\tau - t')(\tau t' - 1)} \, d\tau \tag{3.68}$$

The factor $g_{t'}(t;t_o^{(n-1)}) \frac{1}{t^\tau}$ in Equation (3.67) is a simple algebraic function of t' and $t_o^{(n-1)}$, as can be seen from Equations (2.1) and (3.1); its evaluation at $t' = t_i^{(n)}$ therefore

---

* This subroutine has already been alluded to in the discussion following Equation (3.44). The successive refinement of the Simpson mesh should stop once the density of the Simpson points exceeds that of the points $t_i^{(n-1)}$. Further refinement produces no improvement in the approximation to the integral since the additional integrand values are being obtained by interpolation anyway.

presents no difficulty. On the other hand, because the function $\bar{\beta}(s^{(n-1)}(\tau))$ ordinarily varies very rapidly when the value of $s^{(n-1)}(\tau)$ corresponds to the vicinity of the nose, a special technique has to be used to carry out the τ-integration in Equation (3.68). In this procedure - a so-called adaptive integration subroutine - Simpson's rule is applied separately to various subintervals of the integration interval $-1 \leq \tau \leq 1$. The Simpson mesh-width is made smallest in that subinterval where the integrand is varying most rapidly, etc. The details of this subroutine can be found in [4].

3. The application of the adaptive integration technique requires that certain additional interpolations be performed. The integrand function $\bar{\beta}(s^{(n-1)}(\tau))$ is known only at the points $\tau = t_i^{(n-1)}$ corresponding to the values $s^{(n-1)}(t_i^{(n-1)})$ outputted from the $(n-1)^{st}$ iteration. To evaluate $\bar{\beta}(s^{(n-1)}(\tau))$ at one of the Simpson points, we proceed as follows: denoting by $\tau_{j,n}$ any one of the Simpson points in τ, we first compute $s^{(n-1)}(\tau_{j,n})$ by interpolation among the known quantities $s^{(n-1)}(t_i^{(n-1)})$. Denoting the resulting value of s by $s_j^{(n-1)}$, we find a corresponding value of w through the equation

$$s(w) = s_j^{(n-1)} \tag{3.69}$$

where it will be recalled that the function s(w) depends only on the geometry of the body.

Equation (3.69) is solved - call the solution $w_j^{(n-1)}$ - by interpolation among the quantities w_i, $i = 1,2, \ldots$. We then

compute the function $\beta(w)$ at $w_j^{(n-1)}$ by direct evaluation of the formulas given in Equations (3.27) - (3.29). The resultant number, $\beta(w_j^{(n-1)})$, is the desired value of the integrand function, $\bar{\beta}(s^{(n-1)}(\tau_{j,n}))$, at the Simpson point $\tau_{j,n}$.

Note that by this round-about procedure we have avoided interpolation on a rapidly varying function, viz., $\beta(w)$. [$\beta(w)$ changes rapidly in the vicinity of the nose, $w = 0$.]

4. Although the integrand of the inner integral (see Equation (3.68)) is a continuous function of τ in the interval $-1 \leq \tau \leq 1$, the integrand becomes indeterminate when $\tau = t'$. Evaluation by l'Hospital's rule proves inconvenient because the necessary derivatives with respect to τ cannot be computed with sufficient accuracy. This effect is particularly marked when $t' = \pm 1$, for which case it can be seen that the second derivative of the numerator is required. Accordingly, we evaluate the integrand at $\tau = t'$ by assigning to it the value at a neighboring point. The neighboring point is chosen close enough for the integrand to differ very little from its value at $\tau = t'$ but not so close that the indeterminacy spoils the accuracy of the evaluation. Experimentally it has been found that a separation of about 0.003 between t' and the τ-value of the neighboring point works quite well. The integrand at the neighboring point is computed by interpolation among the points $t_i^{(n-1)}$.

5. The integral on the right of Equation (3.8) has the same form as the inner integral $J^{(n)}(t')$ (Equation (3.68)) except for the replacement of t', which is real, by the complex quantity

$t_o^{(n-1)}$. This removes the aforementioned indeterminacy; otherwise the same considerations apply to the computation of this integral as in the case of $J^{(n)}(t')$.

We conclude this subsection by remarking that the iteration process is terminated in one of two ways. Either a maximum number of iterations is chosen in advance, or else the process stops when a certain convergence criterion is satisfied. The criterion is that

$$\text{Max}\left\{\text{Re}\left(\frac{t_o^{(n)} - t_o^{(n-1)}}{t_o^{(n)}}\right), \text{Im}\left(\frac{t_o^{(n)} - t_o^{(n-1)}}{t_o^{(n)}}\right), \frac{N^{(n)}(1) - N^{(n-1)}(1)}{N^{(n)}(1)}\right\} < \delta \quad (3.70)$$

where the number δ is generally taken to be 10^{-4}. We recall that $N^{(n)}(1)$ is the value at $t = 1$ of the function defined in Equation (3.5).

Inputs to Part C

$$\alpha, \sigma, t_i^{(n-1)}, s^{(n-1)}(t_i^{(n-1)}), \quad i = 1,2, \ldots N_T^{(n-1)}, t_o^{(n-1)}$$

$$n = 1,2, \ldots \quad (N_T^{(o)} = N_R^+ + N_F + N_R^- + 1)$$

Outputs from Part C

$$t_i^{(n)}, s^{(n)}(t_i^{(n)}), \bar{\beta}(s^{(n)}(t_i^{(n)})), \quad i = 1,2, \ldots N_T^{(n)},$$

$$t_o^{(n)}, A^{(n)}, n = 1,2, \ldots$$

D. Computation of Pressure, Force, and Moment Coefficients

The coefficients $C_p^{(n)}[t]$, $c_d^{(n)}$, $c_\ell^{(n)}$, and $c_m^{(n)}$ are computed after each iteration via Equations (3.9) - (3.13). We can effect a convenient simplification of the right side of Equation (3.9) by differentiating Equation (3.5) with respect to t and invoking Equations (3.1) and (3.7). The result is that

$$\frac{f_t(t,t_o^{(n)})}{s_t^{(n)}(t)} = t \exp\left[-\frac{1-t^2}{\pi} J^{(n)}(t)\right] \tag{3.71}$$

where $J^{(n)}(t)$ is the inner integral, Equation (3.68).

It follows that

$$C_p^{(n)}[t] = 1 - t^2 \exp\left[-\frac{2}{\pi}(1-t^2)J^{(n)}(t)\right] \tag{3.72}$$

and since $J^{(n)}(t)$ is computed at the points $t_i^{(n)}$ in the manner already discussed, Equation (3.72) immediately furnishes the quantities $C_p^{(n)}[t_i^{(n)}]$, $i = 1,2, \ldots N_T^{(n)}$. The numerical specification of the function $C_p^{(n)}(s)$ - the normalized pressure as a function of arc length - then results from associating the s-values, $s^{(n)}(t_i^{(n)})$, with the corresponding $C_p^{(n)}[t_i^{(n)}]$, in accordance with the identity

$$C_p^{(n)}(s^{(n)}(t_i^{(n)})) = C_p^{(n)}[t_i^{(n)}] \tag{3.73}$$

The integrands in the integrals of Equations (3.11) - (3.13) are evidently defined numerically at the points $t_i^{(n)}$. We perform the integrations by combining, as previously discussed,

successive applications of Simpson's rule with interpolations among the integrand values. It should be noted that the contents of the curly brackets in the integrands are, for evaluation purposes, replaced by the right side of Equation (3.72), while $s_t^{(n)}(t)$ itself is evaluated by solving for it in Equation (3.71). Finally, the functions $x(s^{(n)}(t))$ and $y(s^{(n)}(t))$ appearing in Equation (3.13) are computed by interpolations among the tables of $x(w_i)$, $y(w_i)$, and $s(w_i)$ that form part of the output of Part A.

Inputs to Part D

$$\alpha, \sigma, t_i^{(n)}, s^{(n)}(t_i^{(n)}), \quad i = 1,2, \ldots N_T^{(n)}, \; t_o^{(n)},$$

$$n = 1,2, \ldots.$$

Outputs from Part D

$$C_p^{(n)}[t_i^{(n)}], \quad i = 1,2, \ldots N_T^{(n)}, c_d^{(n)}, c_\ell^{(n)}, c_m^{(n)}$$

$$n = 1,2, \ldots.$$

4. NUMERICAL RESULTS

In the Introduction, we summarized the results obtained by applying the foregoing computational scheme to four cavitated flows. We now present some of the numerical details. All computations were performed on the IBM 7094 computer.

Case 1. 10-to-1 parabola, zero angle of attack, zero cavitation number.

Inputs: $\alpha = 0$, $\sigma = 0$, $x_A = x_B = 1$, $x_{RF} = x^*_{FR} = 0.015$, $N_R^+ = 30$, $N_F = 100$, $y^{\pm}(x) = \pm \frac{1}{20}\sqrt{x}$,

Maximum number of iterations = 4. Basic flow=flow about wedge.

At the present time, this case is the only one for which there seems to be no possibility of imputing any physical significance to the sequence of computed pressure distributions. As may be seen by referring to Figure 4.1, the distribution corresponding to the first iteration is, to a high degree of accuracy, symmetric with respect to the nose*. This is as it should be since both the basic flow and the true pressure distribution are symmetric. On the other hand, the second and third distributions increasingly show a loss of symmetry, while the fourth distribution bears no resemblance to the first three and in fact is almost antisymmetric with respect to the nose. The corresponding drag coefficients, shown in Table 4.1, vary from one iteration to the next in what seems to be a random manner. (The lift and moment coefficients vanish when the angle-of-attack is zero.)

*The nose in this case is located at s=1.003 since the total normalized arc length for a 10-to-1 parabola equals 2.006. Note that the interval of s-values in Figure 4.1 corresponds to the vicinity of the nose, where the very rapid variations in pressure take place. Outside this interval C_p goes monotonically to zero in all four iterations, as $s \to 0$ or 2.006.

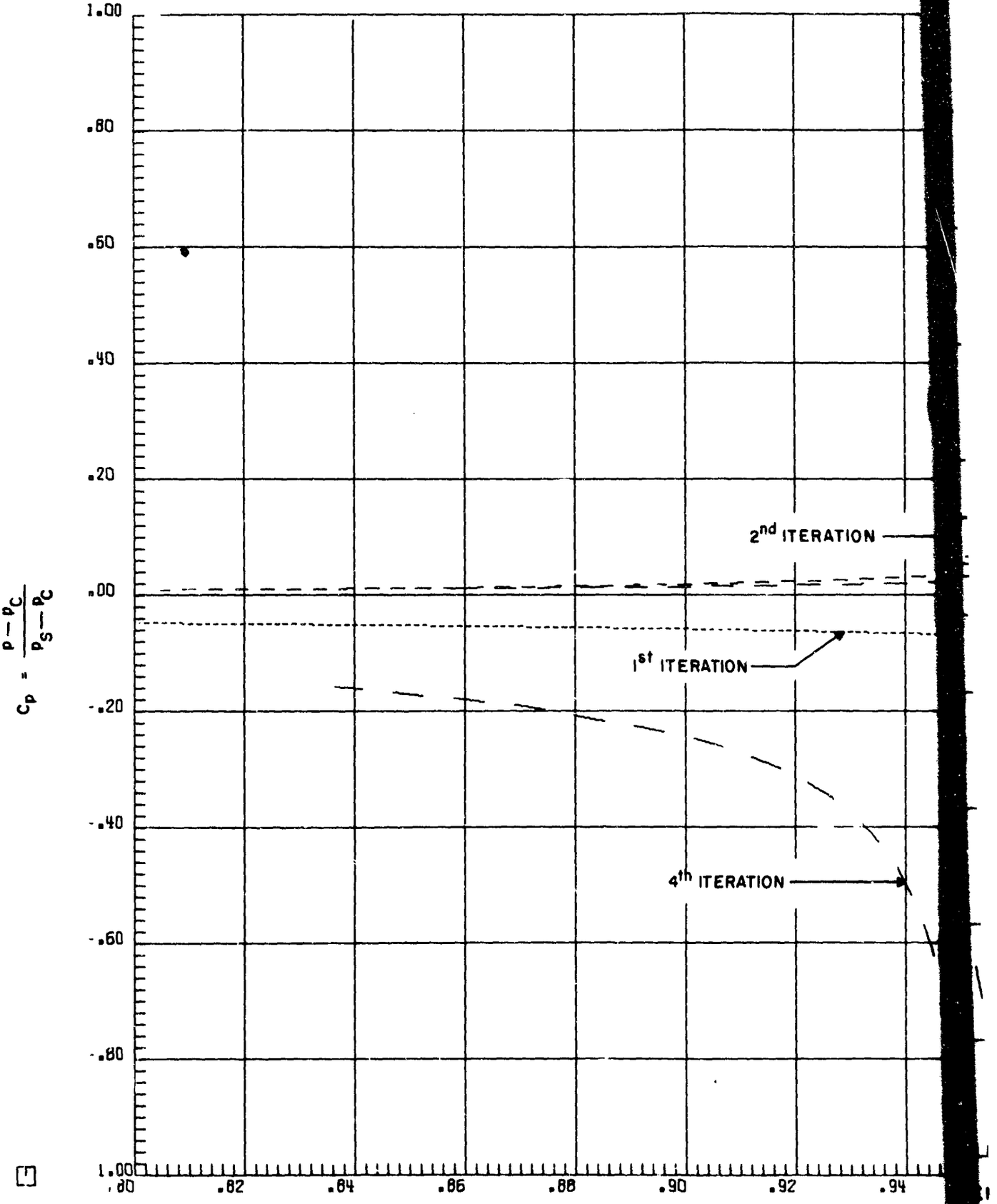
1.00
.80
.60
.40
.20
.00
-.20
-.40
-.60
-.80
1.00
.80
.82
.84
.86
.88
.90
.92
.94
$C_p = \frac{p - p_c}{p_s - p_c}$
2nd ITERATION
1st ITERATION
4th ITERATION
s= ARC LE

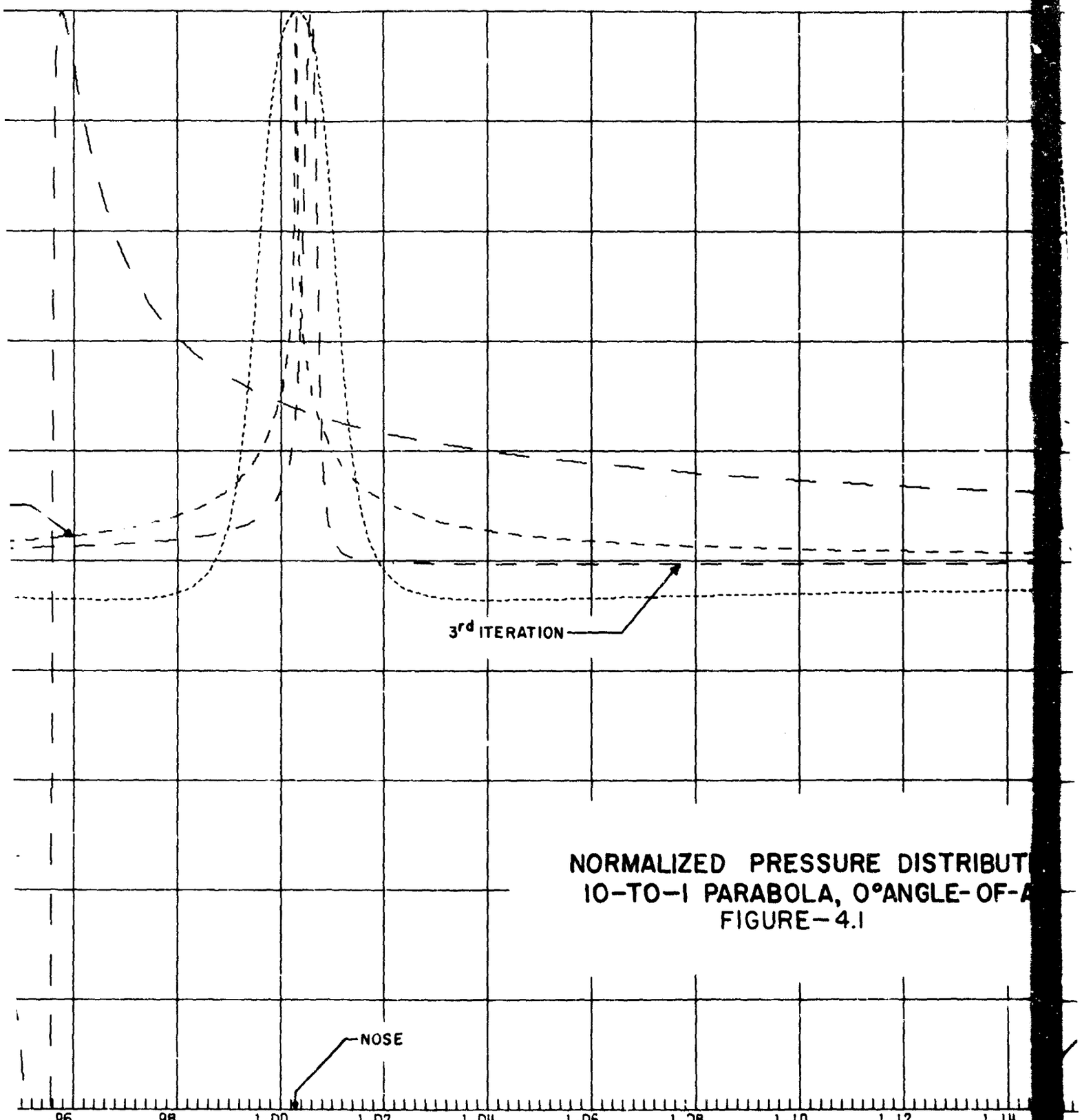

NORMALIZED PRESSURE DISTRIBUT
10-TO-1 PARABOLA, 0°ANGLE-OF-A
FIGURE-4.1

GTH FROM DETACHMENT POINT A

2

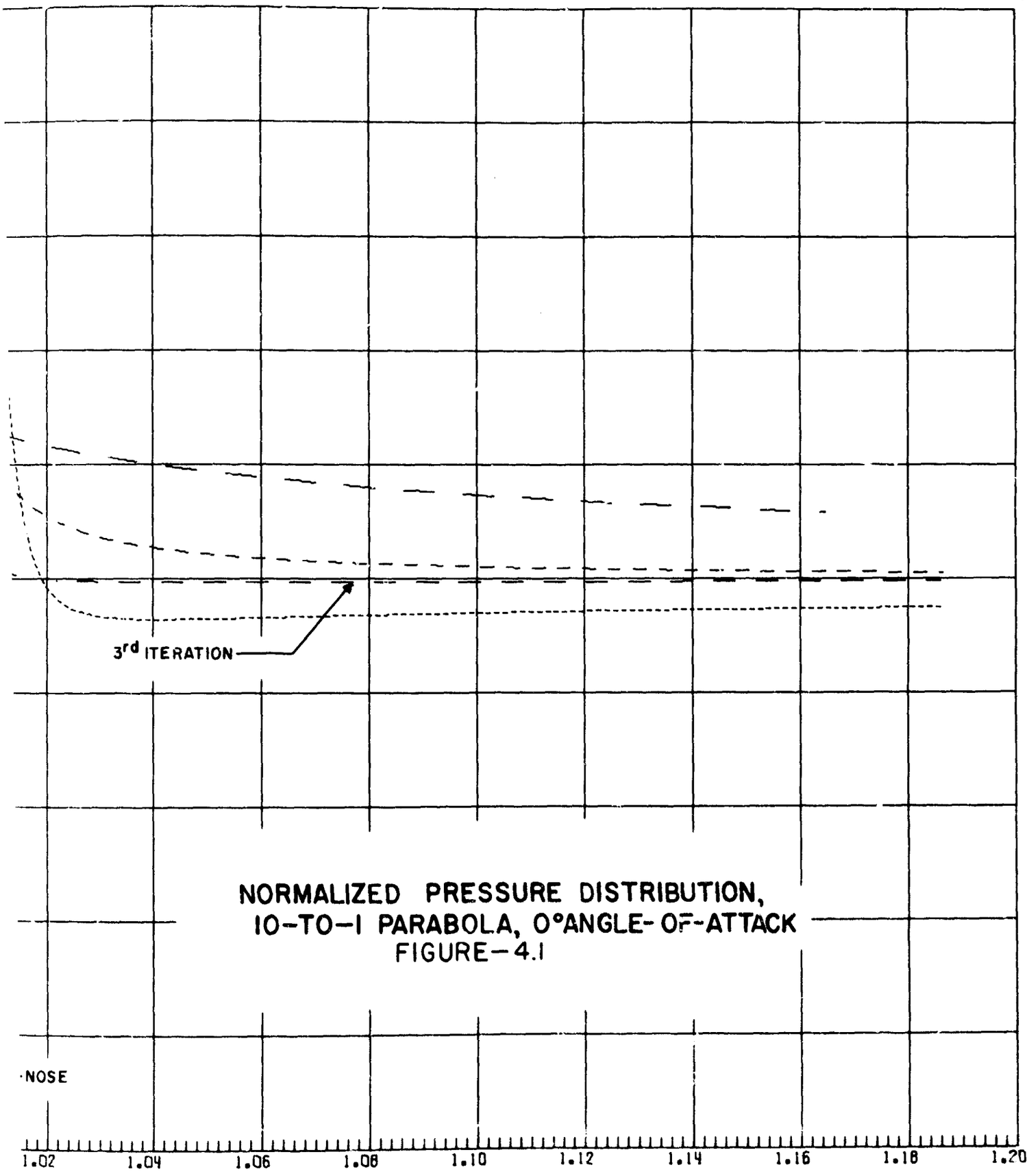

NORMALIZED PRESSURE DISTRIBUTION,
10-TO-1 PARABOLA, 0°ANGLE-OF-ATTACK
FIGURE-4.1

3

TABLE 4.1

Iteration number, n	$c_d^{(n)}$
1	0.00421
2	0.00483
3	0.00301
4	0.00409

A possible explanation of these results is being sought in the fact that for a 10-to-1 parabola, the integrand of the inner integral varies extremely rapidly with τ in the neighborhood of the nose, $\tau=0$, owing to the behavior of $\bar{\beta}(s(\tau))$ in that neighborhood. The behavior is such that the major change in β takes place over a τ-interval of width smaller than that of the fine mesh interval. This abrupt variation could have two consequences: first, it might induce errors in the evaluation of the inner integral; second, it can be shown that the exact value of the inner integral, regarded as a function of t', peaks sharply when t' is in the region where β varies rapidly. Such peaking could then lead to inaccuracies in the computation of the outer integral, owing to the interpolation used to evaluate the outer integrand, $I^{(n)}(t')$.

It must be emphasized that these considerations are hypothetical. The effectiveness of our computational scheme when applied to thin bodies having rounded noses of very high curvature is subject to further investigation.

Case 2. 1-to-1 parabola, zero angle-of-attack, zero cavitation number.

Inputs: $\alpha = 0$, $\sigma = 0$, $x_A = x_B = 1$, $x_{RF} = x^*_{FR} = 0.04$,

$N_R^+ = 15$, $N_F = 40$, $y^{\pm}(x) = \pm \frac{1}{2}\sqrt{x}$

Maximum number of iterations = 7. Basic flow = flow about wedge.

Results for this case are presented in Figures 4.2 and 4.3, and Table 4.2. Figure 4.2 shows the computed pressure coefficient C_p as a function of arc length along the parabola for each of the seven iterations. Since the flow is symmetric about the nose, and the iterates reflect this fact, it suffices to give the pressure distribution over half the perimeter. Note that arc length in this case is measured from the nose rather than from the upper detachment point. The convergence of the iteration process is suggested by the fact that the sixth and seventh pressure distributions differ by at most a few percent (on the graph they are not even distinguishable).

In Figure 4.3 we show a comparison between our final (seventh) distribution and the distribution computed from an approximate formula derived by Johnson[3]. Johnson's formula is meant to apply to parabolas with a higher fineness ratio than one-to-one, but the agreement is still quite close. For the abscissa in Figure (4.3) we have chosen y rather than s because the area under the resultant curve can be shown to equal half the drag coefficient c_d; this expedites the comparison between our drag coefficient and Johnson's, which turn out to equal 0.307 and 0.289 respectively, a difference of less than 6 percent.

Table 4.2 shows how the computed value of $c_d^{(n)}$ varies with the iteration number, n. The sixth and seventh values differ by less than 0.2 percent.

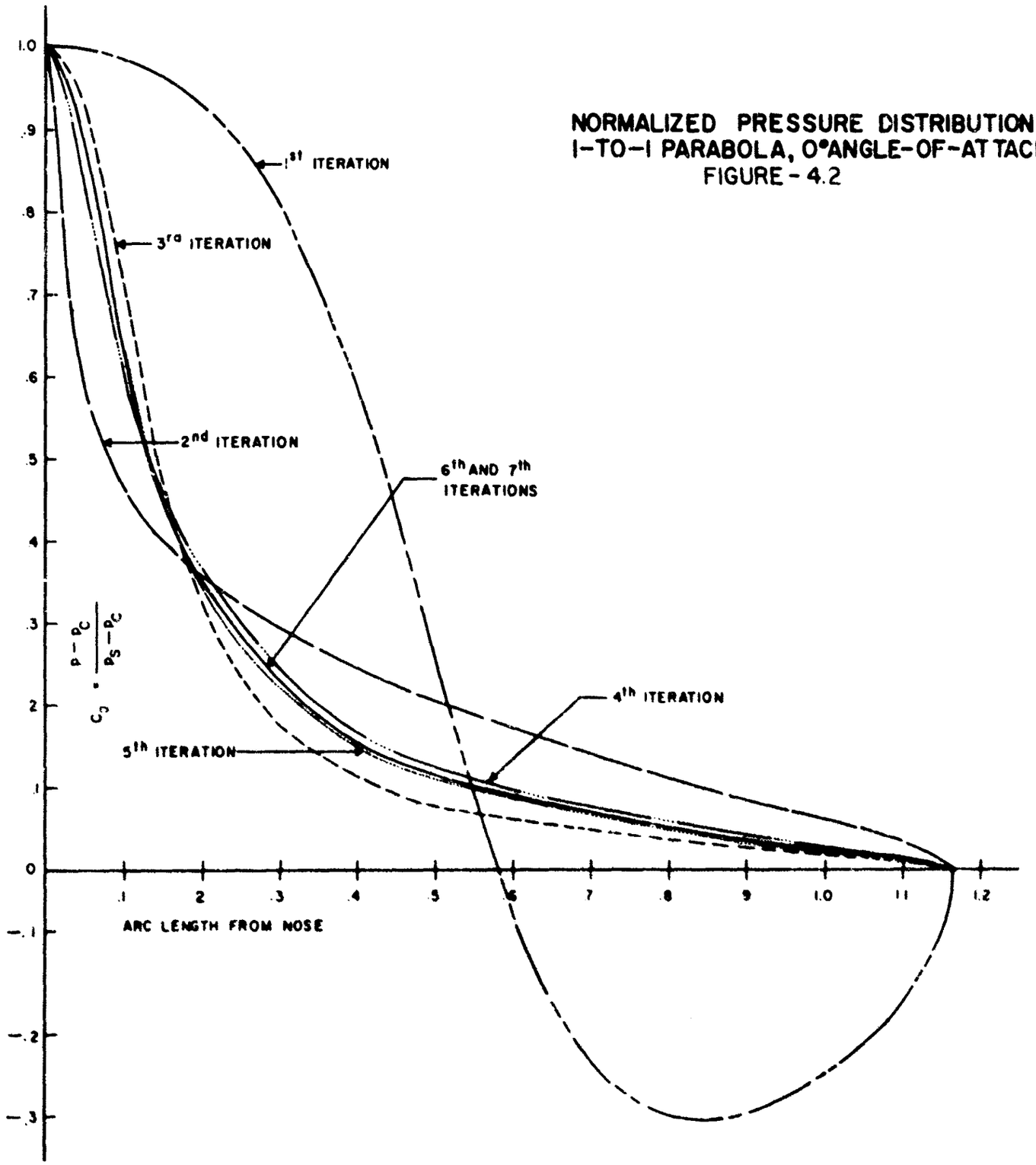

NORMALIZED PRESSURE DISTRIBUTION,
1-TO-1 PARABOLA, 0°ANGLE-OF-ATTACK
FIGURE - 4.2

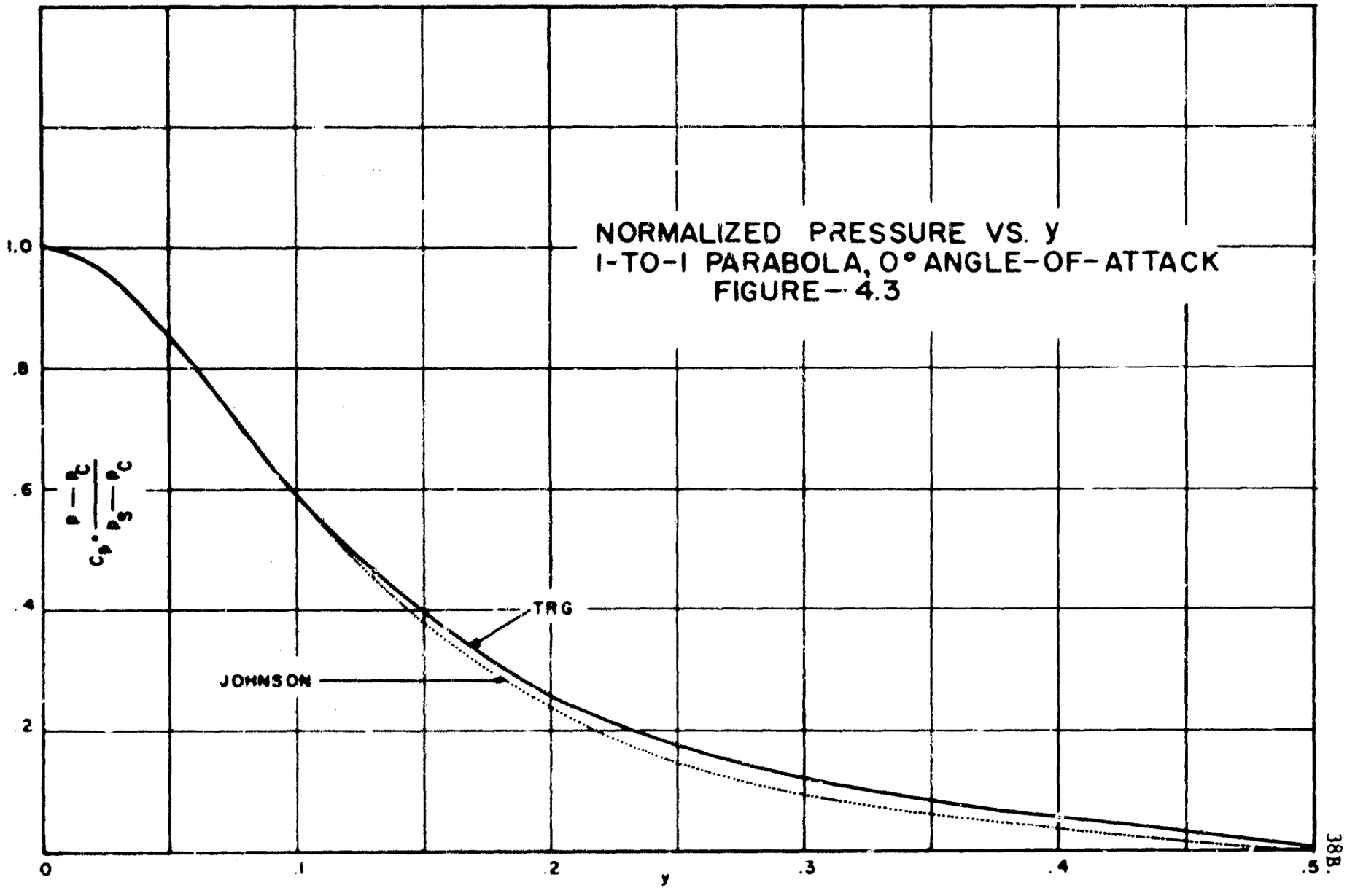
NORMALIZED PRESSURE VS. y
1-TO-1 PARABOLA, 0° ANGLE-OF-ATTACK
FIGURE – 4.3
1.0
.8
.6
.4
.2
0
.1
.2
.3
.4
.5
y
TRG
JOHNSON

TABLE 4.2

Iteration No., n	$c_d^{(n)}$
1	0.44199
2	0.31008
3	0.30353
4	0.30950
5	0.30597
6	0.30734
7	0.30673

Case 3. 1-to-1 parabola, 1° angle-of-attack, zero cavitation number.

Inputs: $\alpha = 1°$, $\sigma = 0$, $x_A = x_B = 1$, $x_{RF} = 0.25$, $x_{FR}^* = 0.10$, $N_R^+ = 15$, $N_F = 120$, $y^{\pm}(x) = \pm \frac{1}{2}\sqrt{x}$.

Maximum number of iterations = 14. Basic flow = flow corresponding to zero angle of attack on same parabola.

This case is distinguished by the fact that for the function $s^{(o)}(t)$ with which the iterations are started, we choose the final iterate, $s^{(7)}(t)$, obtained in the zero angle-of-attack case. Figure 4.4 shows the resulting pressure distributions corresponding to various iteration numbers as a function of arc length measured from the upper detachment point. Note that in the case of a 1-to-1 parabola, S = 2.323. For the sake of clarity, only the first, sixth, thirteenth, and fourteenth distributions are shown. The still considerable separation between the thirteenth and fourteenth distributions indicates that the rate of convergence is much slower than in the zero angle-of-attack case. It can be seen- the curves not shown bear this out - that the pressure distributions

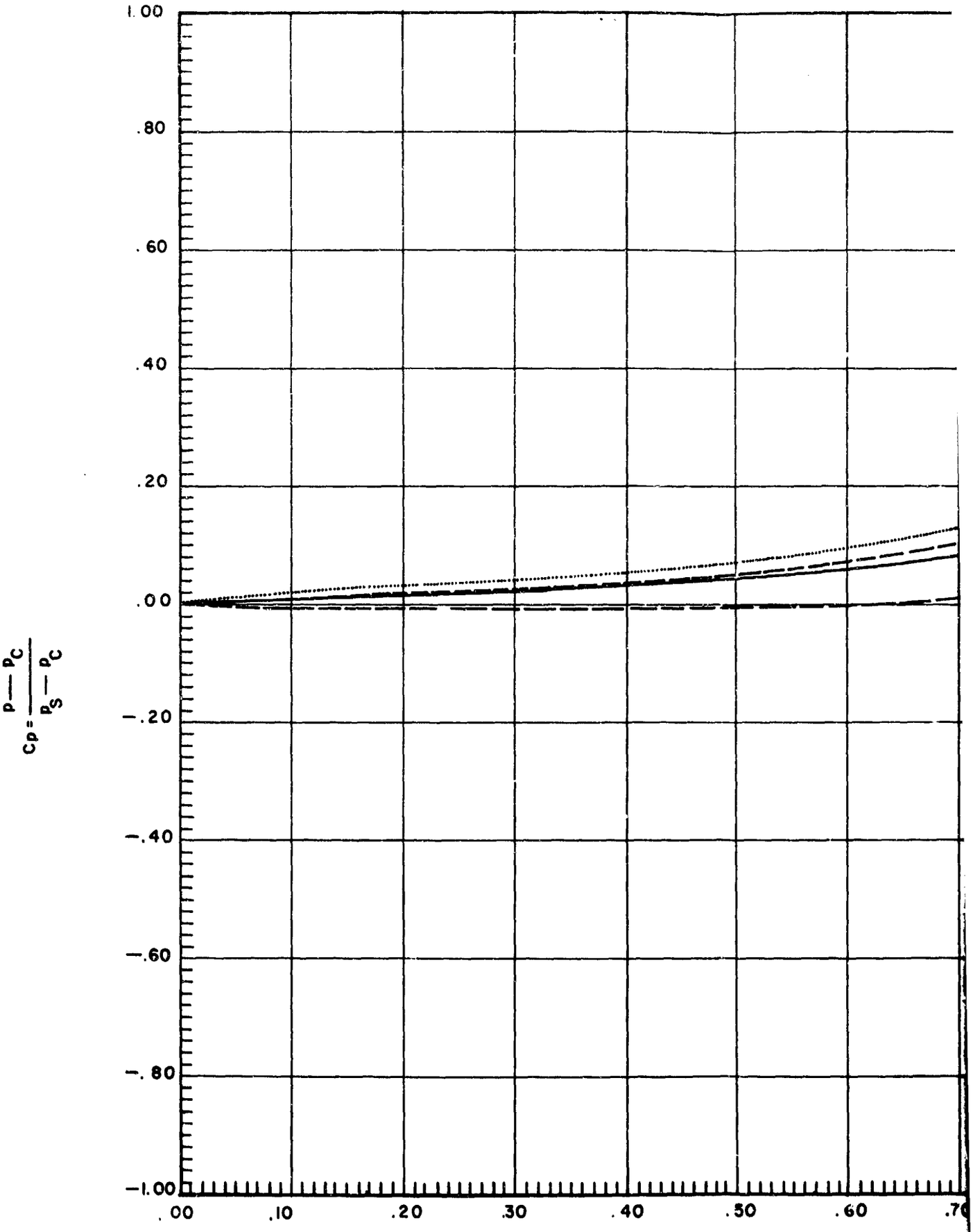
1.00
.80
.60
.40
.20
.00
−.20
−.40
−.60
−.80
−1.00
.00
.10
.20
.30
.40
.50
.60
$C_p = \frac{p - p_c}{p_s - p_c}$

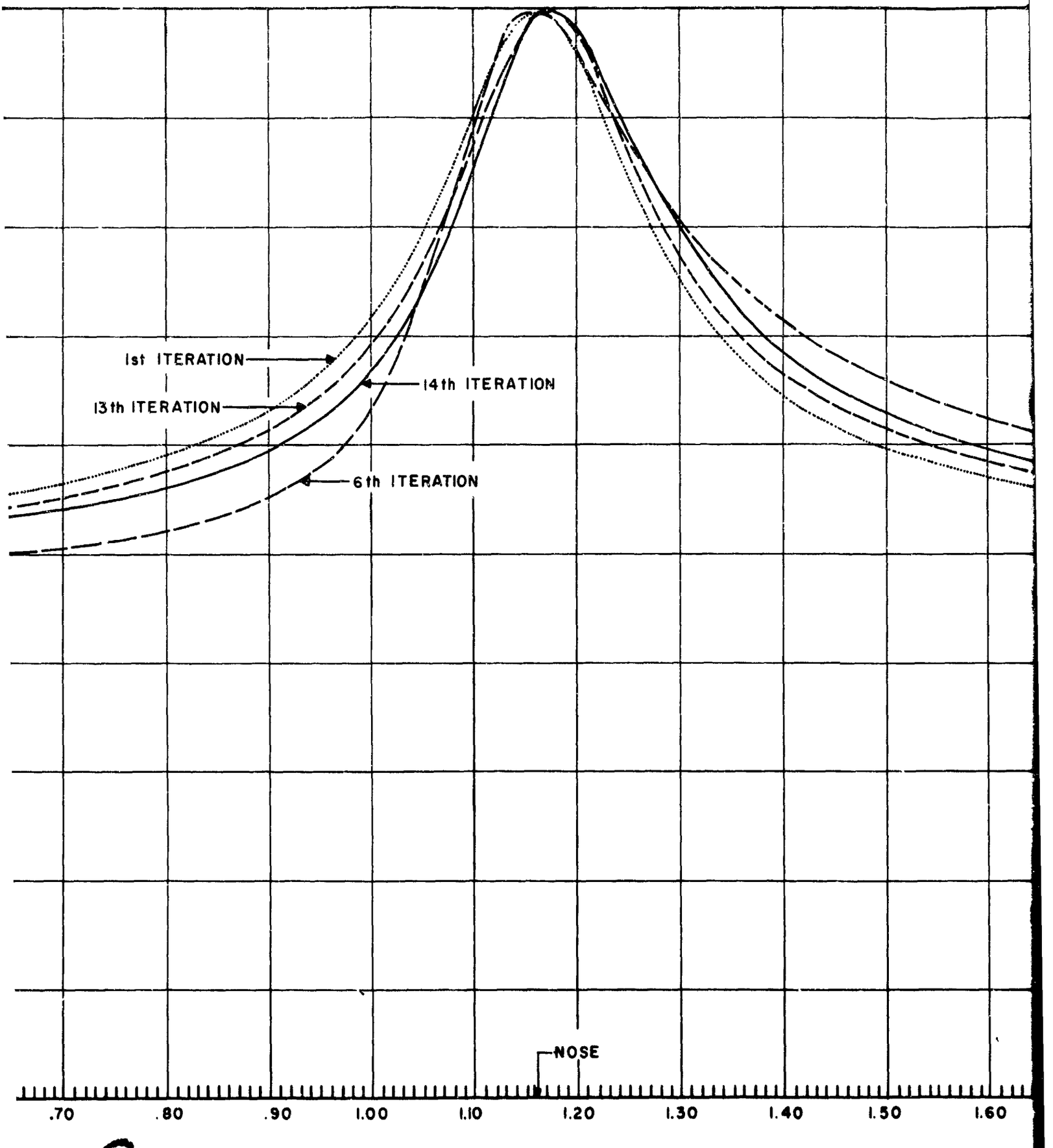
1st ITERATION
13th ITERATION
14th ITERATION
6th ITERATION
NOSE
.70
.80
.90
1.00
1.10
1.20
1.30
1.40
1.50
1.60
s = ARC LENGTH FROM DETACHMENT POINT A

2

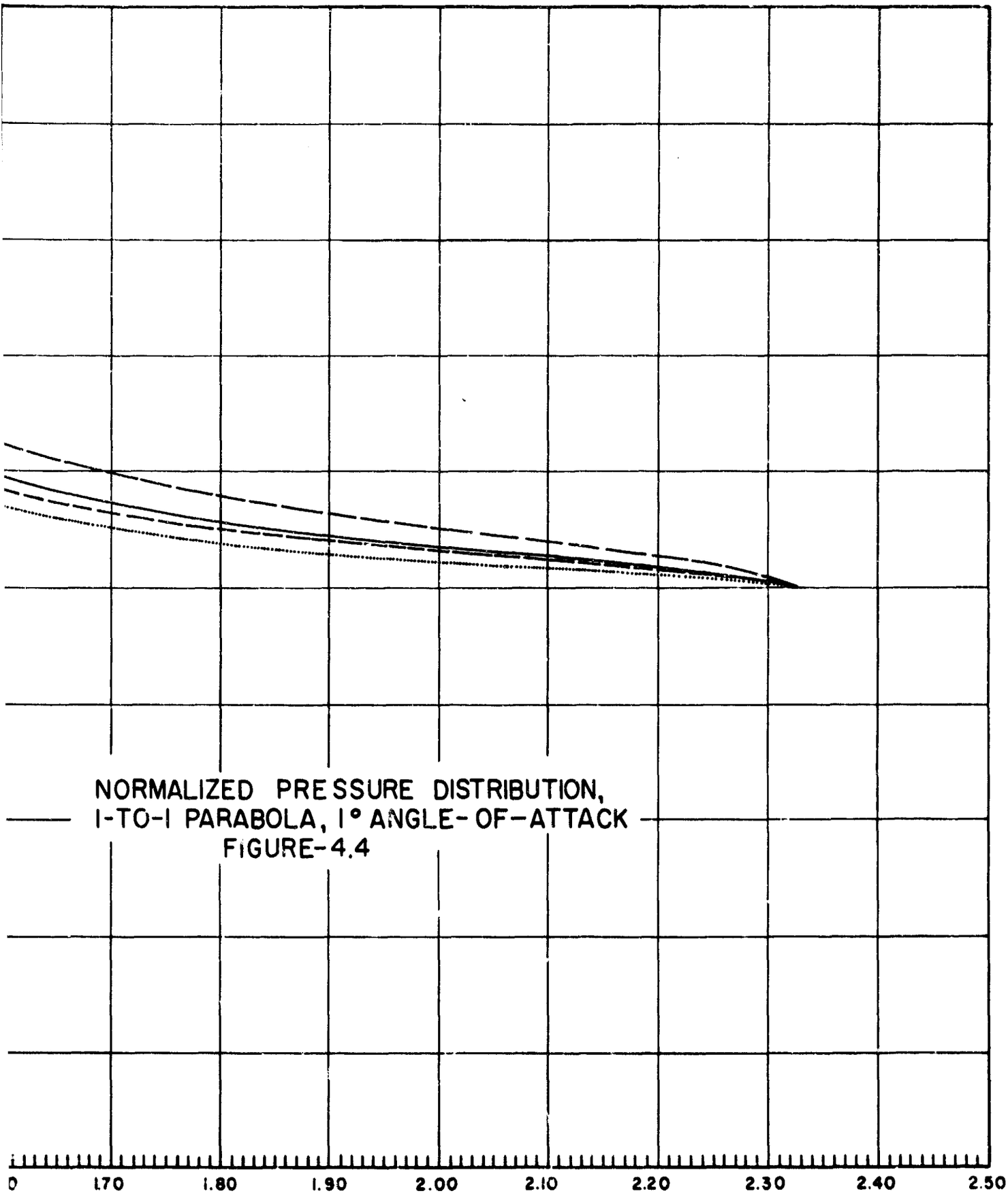

NORMALIZED PRESSURE DISTRIBUTION,
1-TO-1 PARABOLA, 1° ANGLE-OF-ATTACK
FIGURE-4.4

3

shift back and forth as the iteration number changes. A manifestation of this effect is exhibited in Figure 4.5 where we have plotted the s-value of the stagnation point (maximum pressure) as a function of iteration number. The oscillatory behavior is quite apparent, as is the gradual approach to a limiting position.

Table 4.3 gives the computed values of $c_d^{(n)}$, $c_\ell^{(n)}$, and $c_m^{(n)}$ as a function n.

TABLE 4.3

Iteration No., n	$c_d^{(n)}$	$c_\ell^{(n)}$	$c_m^{(n)}$
1	0.30727	-0.00682	-0.00042
2	0.30516	0.03830	0.01172
3	0.30298	0.19697	0.10083
4	0.30795	-0.01678	0.00214
5	0.30488	0.05413	0.02038
6	0.30513	0.15519	0.08022
7	0.30739	0.01061	0.01005
8	0.30577	0.06780	0.02979
9	0.30573	0.12334	0.06427
10	0.30786	0.02816	0.01722
11	0.30571	0.07346	0.03430
12	0.30965	0.10423	0.05441
13	0.30724	0.04170	0.02297
14	0.30585	0.07581	0.03649

The drag coefficient remains substantially constant, apart from a small random fluctuation - rms relative amplitude about 1 percent - apparently due to numerical errors. The

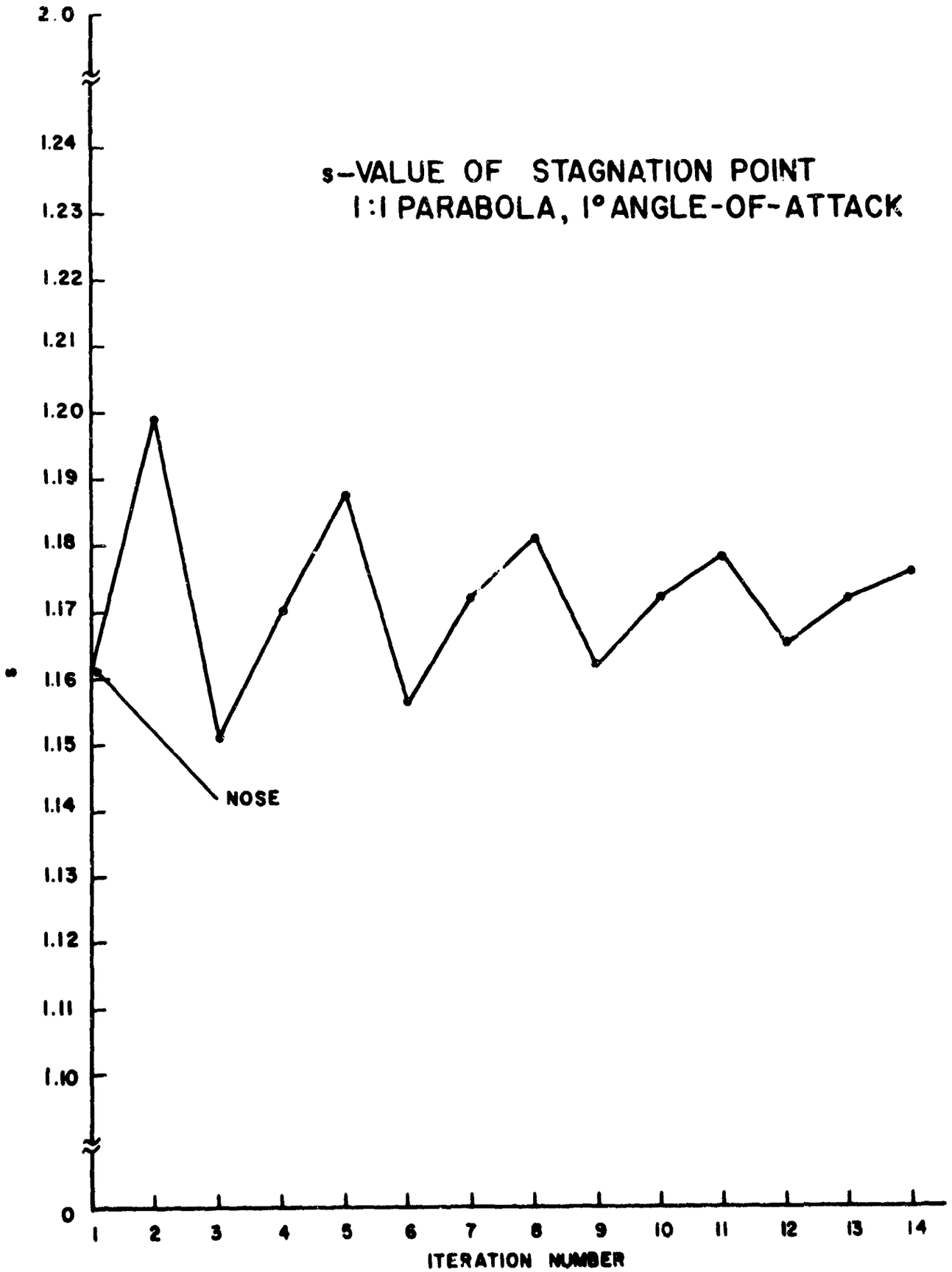
s-VALUE OF STAGNATION POINT
1:1 PARABOLA, 1° ANGLE-OF-ATTACK
2.0
1.24
1.23
1.22
1.21
1.20
1.19
1.18
1.17
1.16
1.15
1.14
1.13
1.12
1.11
1.10
0
NOSE
1
2
3
4
5
6
7
8
9
10
11
12
13
14
ITERATION NUMBER

FIGURE- 4.5

average value of $c_d^{(n)}$ is about the same as the final value in the zero-degree case. The more severe fluctuations in $c_\ell^{(n)}$ and $c_m^{(n)}$ can be explained by referring to Equations (2.5a)-(2.6b). From those equations we see first that when α is small, $c_d \approx c_x$ and $c_\ell \approx c_y$. Thus the computability of c_d and c_ℓ depends on the computability of the integrals in Equations (2.6a) and (2.6b) respectively. Observing that as the integration variable s runs from 0 to S, the angle $\bar{\beta}(s)$ goes from slightly greater than π to slightly less than 2π, we see that $\sin\bar{\beta}(s)$ remains negative over the interval $0 \leq s \leq S$. Since $C_p(s)$ is positive on that interval*, the integrand in Equation (2.6a) is negative throughout; thus there is no cancellation of one part of that integral by the other. On the other hand, the function $\cos\bar{\beta}(s)$ is antisymmetric about $\beta = \frac{3\pi}{2}$ ($s = \frac{1}{2}S$) while $C_p(s)$ is almost symmetric about the same point. It follows that the integral in Equation (2.6b) is the difference between two almost equal quantities, and its computation is therefore highly susceptible to numerical error. This explains why the fluctuations in $c_\ell^{(n)}$ are more severe than in $c_d^{(n)}$. The same argument applies to $c_m^{(n)}$ upon remarking that the terms $x(s)\cos\bar{\beta}(s)$ and $y(s)\sin\bar{\beta}(s)$ in the integrand of Equation (2.5c) are both antisymmetric about $s = \frac{1}{2}S$.

It should be noted, however, that despite the foregoing effect, some tendency toward convergence may be discerned in the tabulated values of $c_\ell^{(n)}$ and $c_m^{(n)}$. In fact, the numbers seem to indicate that as a rough guess, the limiting value of c_ℓ lies

*For a few values of n, $C_p^{(n)}(s)$ goes slightly negative over a short interval in s, but this does not affect the argument.

somewhere between 0.03 and 0.08, while for c_m it lies between 0.03 and 0.06. The need for greater accuracy in computing these integrals is evident.

Case 4. 1-to-1 parabola, 5° angle-of-attack, zero cavitation number.

Inputs: $\alpha = 5°$, $\sigma = 0$, $x_A = x_B = 1$, $x_{RF} = 0.25$, $x^*_{FR} = 0.10$, $N_R^+ = 15$, $N_F = 120$, $y^{\pm}(x) = \pm \frac{1}{2}\sqrt{x}$.

Maximum number of iterations = 14. Basic flow = flow about wedge.

In Figure (4.6) we have plotted the computed pressure distributions corresponding to the first, fourth, ninth, thirteenth, and fourteenth* iterations, the remaining distributions having been omitted for the sake of clarity, as in the 1° case. By contrast with that case, however, there seems to be no trend toward a limiting distribution, and our present opinion is that the sequence of pressure distributions is not convergent. On the other hand, we do not feel that these distributions are meaningless since with the exception of the third distribution (not shown), which has a large negative dip, they are all of the expected form (judging from the 0° and 1° cases), while the computed pressures fall within the expected range. We conclude that the failure to converge is probably the result of fluctuations arising from numerical inaccuracies. As mentioned in the Introduction, this idea is supported by the comparative constancy - rms fluctuation over fourteen iterations about 5 percent-of the drag coefficient as a function of iteration number, n, and by the quite reasonable figure of 0.299 for the

*These were chosen as representative of all fourteen distributions in the range of pressures encompassed.

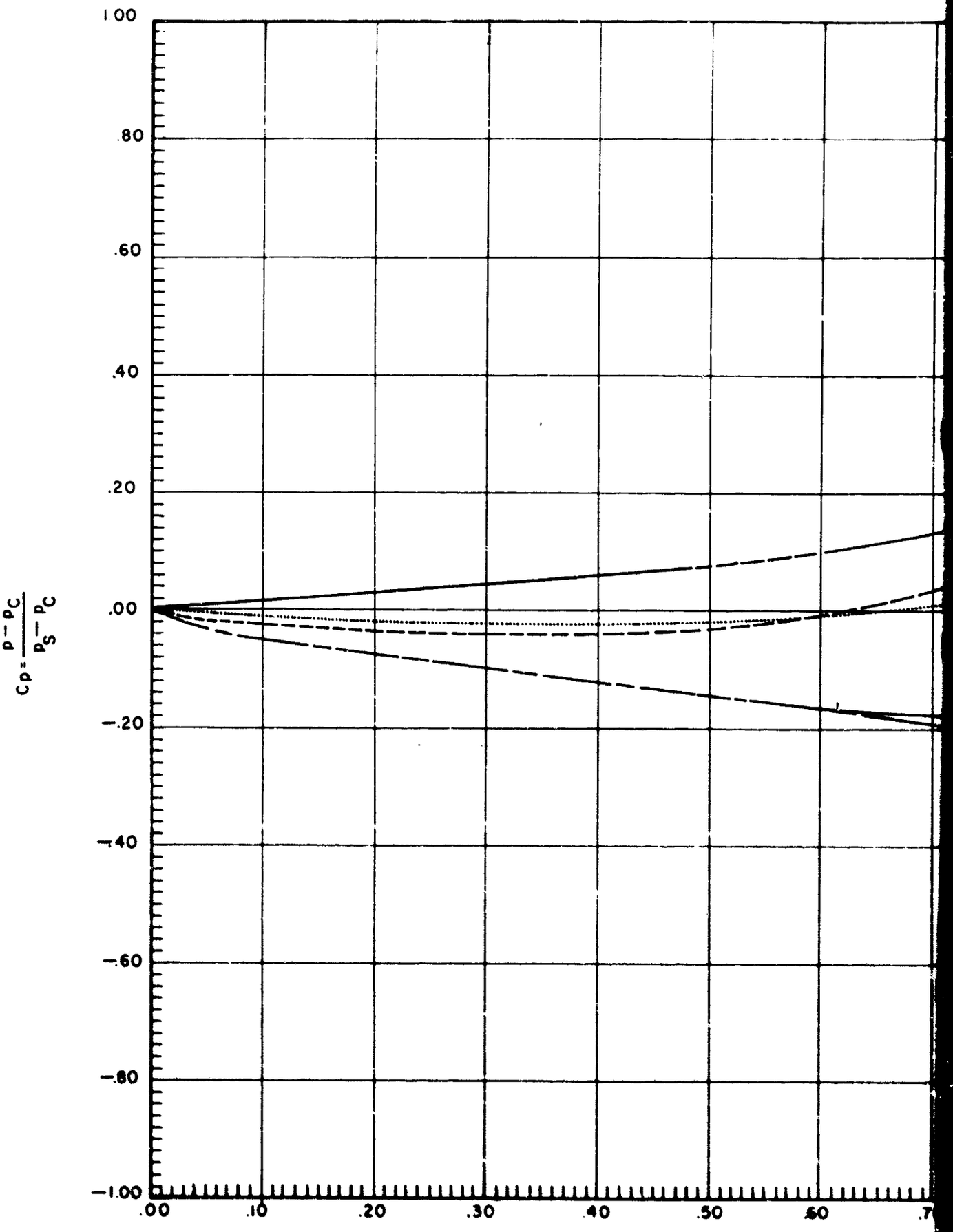
1.00
.80
.60
.40
.20
.00
-.20
-.40
-.60
-.80
-1.00
.00
.10
.20
.30
.40
.50
.60
$C_p = \frac{p - p_c}{p_s - p_c}$

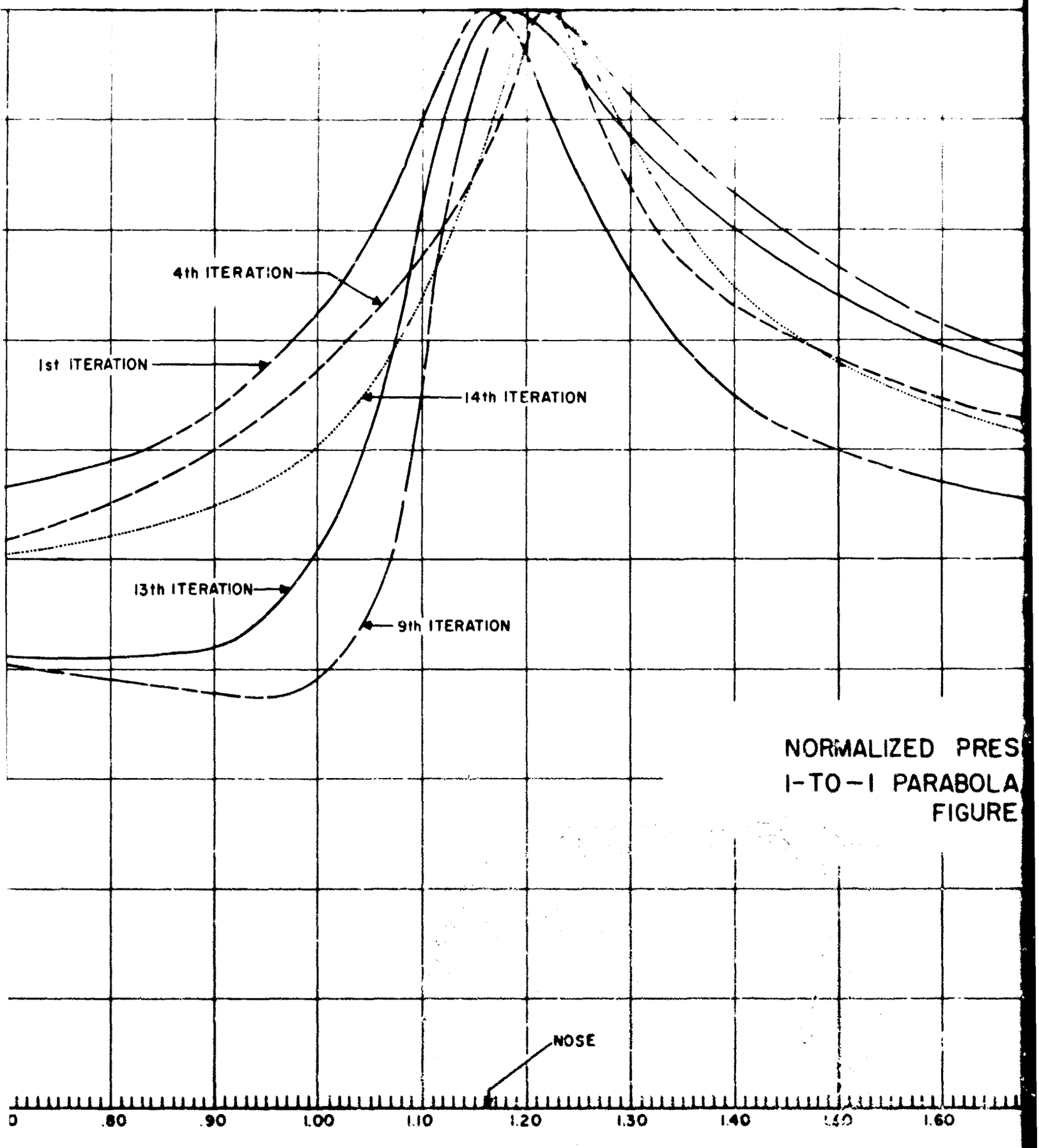

NORMALIZED PRES
1-TO-1 PARABOLA
FIGURE

2

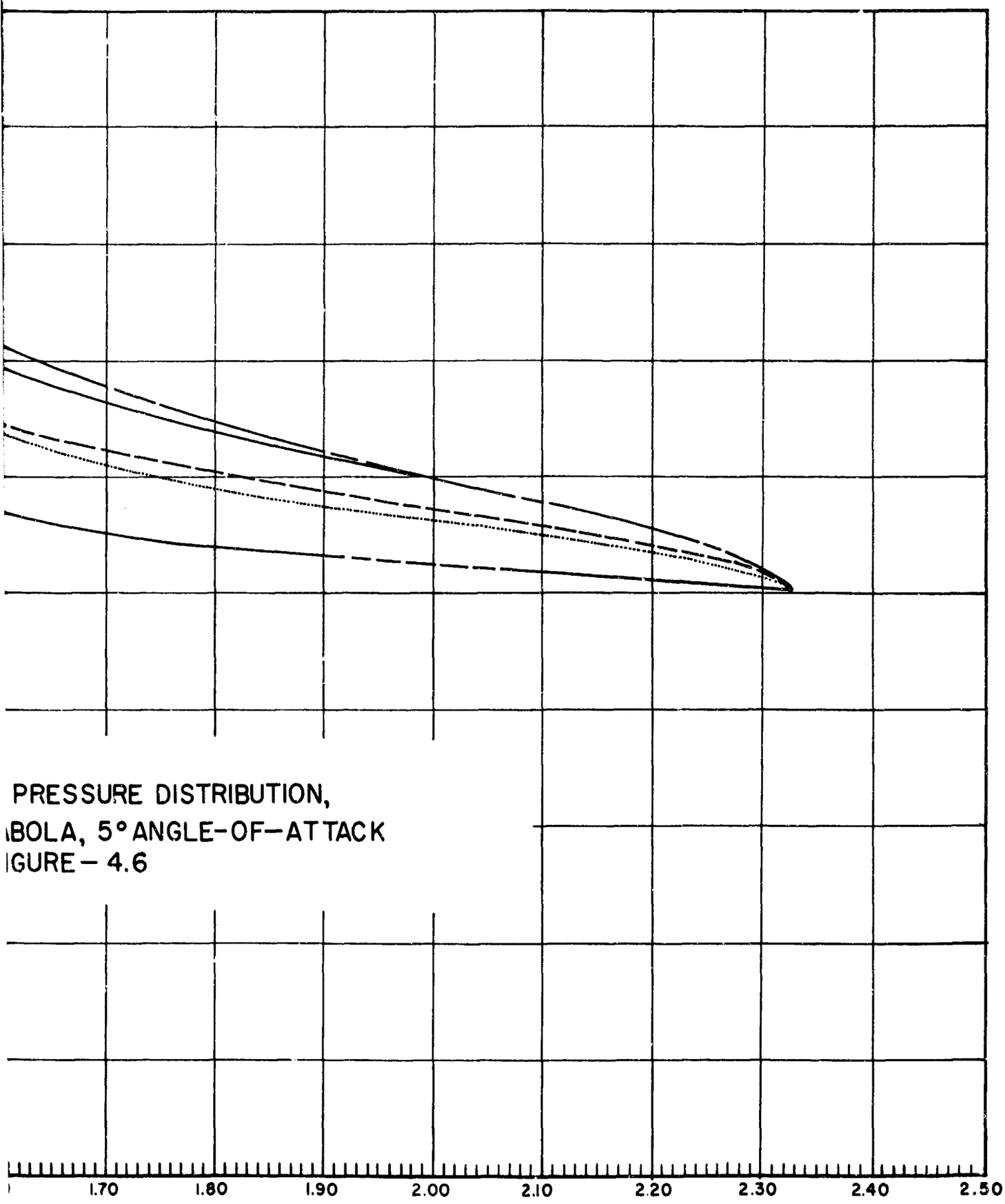

PRESSURE DISTRIBUTION,
BOLA, 5° ANGLE-OF-ATTACK
IGURE – 4.6

3

average over the iterations. The tabulation of these values and the corresponding values of the lift and moment coefficients is exhibited in Table 4.4.

TABLE 4.4

Iteration No., n	$c_d^{(n)}$	$c_\ell^{(n)}$	$c_m^{(n)}$
1	0.30568	-0.02721	-0.00028
2	0.28080	0.14818	0.05413
3	0.22256	1.04143	0.50903
4	0.32191	0.17081	0.10733
5	0.29101	0.36652	0.17795
6	0.29054	0.34706	0.17524
7	0.29248	0.50943	0.25906
8	0.30700	0.22710	0.11964
9	0.28604	0.45990	0.22614
10	0.31108	0.29812	0.16118
11	0.29963	0.27486	0.13723
12	0.28485	0.42457	0.20862
13	0.30755	0.39021	0.20712
14	0.30790	0.19595	0.10319

Note the much larger values of $c_\ell^{(n)}$ and $c_m^{(n)}$ in the case of the 5° angle-of-attack as compared with the 1° case. This was to be expected and further substantiates our opinion that the 5° pressure distributions have some physical significance.

5. SUPPLEMENTARY DISCUSSION AND RECOMMENDATIONS

As evidenced in this report, our experience with the computation of pressure distributions by application of Wu's theory of cavitated flow suggests several steps that might be taken to improve our technique.

1) Since, in our opinion, the numerical inaccuracies in the various integrals are probably the principle cause of those anomalous results already described, a major effort should be made to improve the accuracy of the integration process. The most direct way of doing this is simply to increase the number of data points, especially in the fine mesh region. The only limitation on the improvement in accuracy thus attainable is the possibility of excessive computation time. However, the cases already run have used less than 0.01 hours per iteration on the IBM 7094, so that we seem to have considerable leeway in this respect.

2) It is possible that in the 5° case there is an additional factor tending to prevent convergence. Specifically, the basic flow, which in that case was the flow about the wedge at 0° angle-of-attack, may be too far removed from the actual flow. This suggests that one might proceed stepwise by using the 0° solution for the parabola as the basic flow in the 1° case, the 1° solution as the basic flow in the 2° case, etc., thereby "creeping up" on the situation of a 5° (or higher) angle-of-attack. Naturally the increments in the angle-of-attack could be made smaller if this was thought desirable.

3. An increase in the rate of convergence of the iteration process might be effected through some technique for processing the iterates in a manner more sophisticated than successive substitution into the integral of the integral equation. For example, a simple and familiar technique of this kind consists of substituting into the integral not the last iterate, but the average of the last two. Apparently this has been found to work quite well in some cases. Variations of this idea, as well as more elaborate procedures, could also be tried.

REFERENCES

1. T. Yao-tsu Wu, A Wake Model for Free-Streamline Flow Theory, Part I, (Engineering Division) California Institute of Technology, Report No. 97-2, September 1961.

2. T. Yao-tsu Wu and D.P. Wang, A Wake Model for Free-Streamline Flow Theory, Part II. Cavity Flows Past Obstacles of Arbitrary Profile, Hydrodynamics Laboratory, Kármán Laboratory of Fluid Mechanics and Jet Propulsion, California Institute of Technology, Report No. 97-4, May 1963.

3. S.E. Starley and V.E. Johnson, Jr., The Design of Two-Dimensional Low-Drag Base-Vented Struts, Hydronautics, Inc. Technical Report 001-11, page 10, March 1962.

4. W.M. McKeeman and Larry Tesler, "Algorithm 182. Nonrecursive adaptive integration," Communications of the ACM 6, No. 6, page 315, June 1963.